Markou, Athanasios; Elmas, Serenay; Filz, Günther H.

Revisiting Stewart–Gough platform applications: A kinematic pavilion

Published in:
Engineering Structures

DOI:
10.1016/j.engstruct.2021.113304

Published: 15/12/2021

Document Version
Publisher's PDF, also known as Version of record

Engineering Structures 249 (2021) 113304

Contents lists available at ScienceDirect

Engineering Structures

journal homepage: www.elsevier.com/locate/engstruct

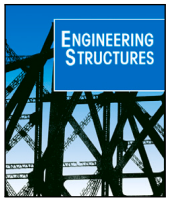

Revisiting Stewart–Gough platform applications: A kinematic pavilion

Athanasios A. Markou [a,*], Serenay Elmas [a,b], Günther H. Filz [a,b]

[a] Department of Civil Engineering, Aalto University, Espoo, Finland
[b] Department of Architecture, Aalto University, Espoo, Finland

ARTICLE INFO

Keywords:
Stewart–Gough platform
Transformable architecture
Kinematic structure
Stability
Structural design

ABSTRACT

Stewart–Gough platforms are well known for their extraordinary kinematic motion and therefore they are widely used as devices, ranging from flight simulators to microsurgical manipulators. However, they have not yet been explored much as architectural objects and transformable spaces with regards to irregular arrangements of legs and their associate structural performance. In the current study, an innovative architectural and structural application of the Stewart–Gough platform, implemented as full-scale kinematic pavilion, namely the Zero Gravity pavilion, at Aalto University, Finland, is presented. During the design process a Stewart–Gough 3–3 configuration was rearranged to an irregular 6–6 configuration. The architectural freedom in the arrangement of columns was guided by its immanent effect on the structure's motion, stability, and strength. We opted for one telescopic leg only and its selection is based on four main criteria. Firstly, for each telescopic leg the stability of the different configurations is investigated. Secondly, the self-collision of leg–leg, leg–roof, and roof–floor was investigated by means of physical and computational models as well as through the full-scale pavilion. Thirdly, the selection process is influenced by the force distribution on the six legs. Fourthly, the path trajectory of the kinematic structure is examined in terms of magnitude and type of motion as an architectural feature. The final choice of the telescopic leg was based on the conclusions drawn from the parametric architectural and structural studies. The overall spatial and structural qualities of the system was validated by the full-scale Zero Gravity pavilion.

1. Introduction

1.1. Stewart-Gough platform applications

In 1955, an automobile stability device was built in Dunlop Rubber Co. [1], which was described thoroughly in 1962 by V.E. Gough and S.G. Whitehall [2]. The system consists of two platforms, a fixed and a moving one, joined by six loading jacks, acting as legs, with gauges connected through universal joints at both ends. The device allows for a wide range of motion of the wheel mounted on the moving platform in order to investigate tyre wear and tear.

When in 1965 D. Stewart, who was working for Elliott Automation Co., tried to publish his work on flight simulators [3], Gough was one of the reviewers [4]. It turned out that Stewart was unaware of Gough's and Whitehall's work, which is similar regarding the kinematic behavior but mechanically different, [1]. The moving platform is supported by three articulated legs comprised of hydraulic jacks. Each one of those legs is constrained by another jack, which is connected to the body of the legs creating a shape similar to a 90° counter-clockwise rotated letter λ.

At the same time with Stewart in 1964, an engineer from the Franklin Institute, namely K. Cappel, filed a patent for a helicopter flight simulator, which was approved in 1967 [4] similar to Gough's and Whitehall's device. In this case, the arrangement of the six legs and two platforms creates an octahedron.

Gough, Whitehall, Stewart and Cappel established the basis of the 'Stewart-Gough platform' (SGP) research topic within the field of parallel coupled 6-DOF manipulators [4], even though their theoretical background dates back centuries [5]. Since then, a wide range of SGP applications has been presented from various scientific fields mainly due to their accuracy, rigidity and adaptability [6]. Typical configurations of the leg[1] arrangements of the SGP can be classified as 3–3 and 6–3, as shown Fig. 1.

More specifically, Morán et al. [7] modified the original SGP by restricting the linear motions along x and y axes to reduce economic costs. The modification resulted in a system with four degrees of

* Corresponding author.
E-mail address: athanasios.markou@aalto.fi (A.A. Markou).

[1] Since our research concentrates on architectural applications paired with structural design, in our further explanations the term "leg" and "column" will be equivalently used depending on the intended focus.

https://doi.org/10.1016/j.engstruct.2021.113304
Received 26 January 2021; Received in revised form 12 September 2021; Accepted 28 September 2021
Available online 26 October 2021

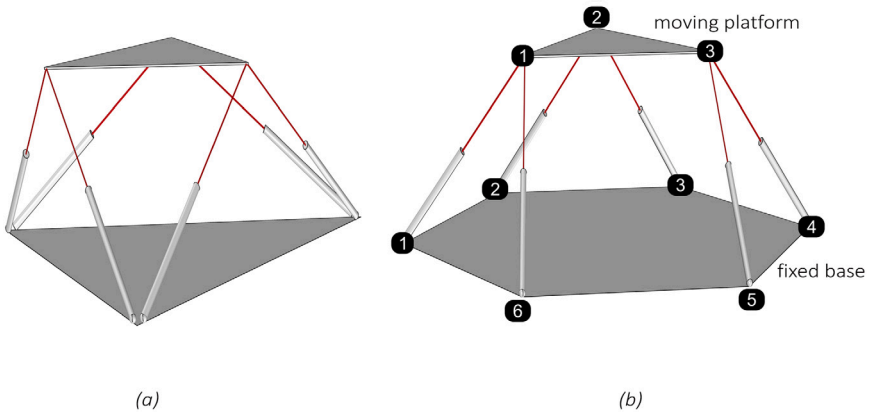

Fig. 1. (a) 3–3 and (b) 6–3 configurations of Stewart–Gough platform.

freedom (DOF), instead of six. The purpose of the work was to develop a rotating platform able to recreate the disorientation effects of the pilots due to centripetal accelerations, which result in optical illusions. Along the same lines, Copeland et al. [8] built a full-scale prototype flight simulator for pilot training. The cockpit consists of a sphere based on Mecanum wheels without joints, which provide unbounded orientation workspace, while the translational actuation is provided by an SGP. In another attempt towards motion simulators, Advani et al. [9] suggested an SGP to replace the current gimbaled system in the Vertical Motion Simulator for NASA. Furthermore, Campos et al. [10] developed an active helideck system that allows helicopters to land on floating structures (e.g. ships) by limiting the movements of the landing platform based on a 3–6 SGP. Additionally, Ross et al. [11] used an SGP to simulate the motion of a ship stern in order to provide surge, pitch, heave and roll to test a zero visibility autonomous landing algorithm for unmanned aerial vehicles (UAV).

Liu and Wiersma [12] used a 3–3 SGP to support patient's head during radiosurgery in order to minimize the exposure of normal tissue to radiation [13]. Furthermore, Akcali et al. [14] suggested an SGP as an external fixation for bone fractures. The proximal and distal fragments are attached to two ring platforms connected with six legs [15]. Sevillano et al. [16] suggested a 3–3 SGP as a human gait simulator. The device is used to study the human gait to treat patients from motor injuries. In the same manner, Kalani et al. [17] used an SGP to simulate the human jaw system. Yang et al. [18] used an SGP miniature as active microsurgical manipulator. The device involves linear motors that provide a 4 mm by 4 mm workspace [19]. Along the same lines, Wapler et al. [20] suggested a 3–3 SGP for precision surgery. In order to achieve positioning accuracy of 10 μm the authors suggest a teleoperated SGP operated by a man–machine interface system. Similar devices have been suggested for skull surgery by Kobler et al. [21], where the SGP is attached to the patient's skull to improve accuracy. Furthermore, Park et al. [22] suggested the use of SGP systems to correct the posture of the human spine. The authors used two 3–3 SGP systems in series with independent control of force and position.

Reinoso et al. [23] used parallel platforms to construct a climbing robot around tubular structures, such as pipes, bridge cables, towers and trunks. The six legs of the 3–3 SGP connect the two circular rings and allow climbing outside or inside tubular structures. Galvan-Pozos and Ocampo-Torres [24] suggested a new wave energy converter based on the SGP concept. The authors propose a 6–3 SGP, where three rigidly interconnected floats form an equilateral triangle, namely the upper platform, which is connected to the fixed base. Each leg consists of a linear electrical generator, which driven by the motion of the upper platform due to wave motion, produces energy. Another application in marine structures is the floating marine platform studied by Horoub et al. [25], which forms a 3–3 SGP connected to the seabed with six mooring cables allowing for three DOF motion.

Stewart–Gough platform has also been used in radio-telescopes to control the position of its secondary mirror [26,27]. More precisely, Yingjie et al. [28] tested a feed positioning system for a 500 m aperture radio-telescope. The system comprises three components, namely a cable system, a trolley hanged on the cables and an SGP mounted on the trolley. The SGP acts as a vibration isolator mainly from wind disturbances, isolating the trolley-cable system from the lower platform, see also [29]. Likewise, Premont et al. [30] suggested an active isolation system for space applications. The system consists of a 3–3 SGP with active isolated legs, to avoid low amplification at resonance and large attenuation at high frequency provided by passive systems [31,32]. Iqbal et al. [33] studied the dynamics of SGP subjected to moving payload to investigate the behavior of satellite antennas with movable dishes.

Richter et al. [34] proposed the use of an inverted 3–3 SGP, which can be mounted to a crane to create a suspension and positioning tool on the construction site. The legs consist of six cables and the upper platform comprises three telescopic arms. Additionally, Salah et al. [35] used a similar SPG with cable-legs to build an automated storage and retrieval system for warehouses, see also [36]. In another application for the construction field, Kim and Bernold [37] used a 3–3 SGP for handling and joining heavy pipe segments to increase safety and accuracy. Despite the hard control interface compared to the conventional electric winch and cable method, the SGP system provided sufficient accuracy during the pipe manipulation. Stewart–Gough platform has also been used for material handling and characterization [38,39]. Additionally, Hansen et al. [40] proposed a mobile 3–6 SGP for machining components of the wind industry in a flexible process. The machining unit provides the possibility of different configurations to reduce its workspace.

1.2. Stewart-Gough platform as an architectural object

The historical review implemented in the previous section, puts some light on the diverse application possibilities of SGP within a wide variety of fields. In common use, an SGP is a parallel robot that consists of a mobile rigid platform, which is connected to a fixed base by six articulated legs as illustrated in Fig. 1, frequently investigated in literature with well-established design [42–44]. Each of the legs, which typically have the same kinematic structure, is connected to the platform and the base by universal joints at points that are distributed in a geometrically symmetric way [22]. Therefore, the legs are commonly arranged in symmetric constellations of (isosceles) triangles forming 3–3 or 6–3 configurations as shown in Fig. 1. In this paper such leg-arrangements are, not least from an architectural point of view, referred to as regular designs. In contrast, irregular

Fig. 2. Zero Gravity 2.0 exhibition in Espoo, Finland, [41].

designs are referring to leg-arrangements with all legs skew. Regular designs characterize the majority of application-related setups, which usually aim at a maximum workspace [45] and for ensuring the desired stability and functionality [46] of the mechanism such as achieving predefined paths, and to reach certain points or workspaces.

In the field of parallel robots the terminology of architecture, structure, modeling, and design is predominantly used to describe the components, joints and configuration of such systems and also to highlight the differences between different approaches such as parallel and/or serial robot settings with different DOF's [47]. Inhere, architecture is referred to as both, the process and the product of conceptualizing, designing, planning and constructing structures with the aim to fulfill practical and expressive requirements, and thus it serves both utilitarian and aesthetic ends. Structure is a key aspect of architecture as a load-bearing, functional requirement and as an aspect of its safety. In this context architectural works, in the material form of built structures or as works of art, are often perceived as cultural symbols and expression of society.

Nowadays, we are on the move from a purely static thinking about architecture towards a more dynamic perception and idea of our built environment. In the light of present environmental and societal challenges, dynamically changing systems, building envelopes, and spaces beyond the scale of technical equipment can be of interest for architecture and engineering.

Kinetic architecture [48] and transformable design, adaptive and adaptable architectural spaces [49] can be seen as emerging topics in the field of innovative architectural and structural design [50,51]. The concept of buildings that can reposition parts of their structure to change their appearance, to create different usable spaces or to respond to environmental conditions is of interest to architecture for long time. The "velarium" [52] of the Colosseum in Rome, Italy can be considered an early example of kinetic architecture. In 1924, architect Konstantin Melnikov proposed a five-story building, four floors of which revolve around a fixed core, in a competition for the construction of the Moscow branch of the Leningrad Pravda newspaper, [53,54]. Other trends focus on spatial optimization [55], on touristic attractions [56], and on multi-functional design [57] by applying transformability to different scales from mobility concepts [58], to spatial configurations [59], to furniture.

During past decades, advancements in mechanical, electrical systems and robotics are opening up new frontiers with a focus on responsiveness and sustainability aspects. The integration of sensing and responsive technology systems pervades the architectural discourse. Self-regulating technological systems can regulate temperature, light, energy, safety, and other conditions. Even though the Villa Girasole [60,61] was probably the first building to follow the course of the sun, recent projects increasingly focus on the buildings' envelope. Pioneering examples include the Institut du Monde Arabe, 1987, [62], the Al Bahr Towers in Abu Dhabi [63–65] and the Penumbra system, 2014 [66], among others. Conversely, there exists a long genealogy of buildings that uses transformative and mobile elements to control the same set of comfort factors by means of analogue control compared to their above-mentioned high-tech counterparts. These kinetic elements regulate the environmental conditioning of the interior as a fundamental design objective. The House With Balls, 2009, the Social Pavilion, 2006 [67], the Snowcone, 2015 [68] and the Shiver Pavilion, 2015 [69], among innumerous other projects can be seen in this context, where at a scale of a panel or a wall slide, fold, pivot and transform the building climatically and visually.

Even though the combination of sensors, processors and effectors of the movable, responsive or adaptable elements transform the perception and understanding of architecture from static into actively changing configurations [70], the mechanism itself and as it changes over time has only recently come into the focus of interest and consideration [71]. The well-known, geometrical principles for stable trussed bearing structures which can also be folded by Santiago Calatrava [72] and the expanding structures of Chuck Hoberman [73] in the field of kinetic art have triggered new applications in engineering like tensegrity bridges [74] and scissor systems [75], in robotics and deployable mechanisms [76], in material sciences and nanotechnology [77] and in computational geometry and motion processing [71] among other fields.

Altogether, most of the mentioned projects and examples mainly or exclusively focus on the effects of the mechanisms. Conversely, mimicking the visual appearance of a 6–6 SGP with its separated, pinned legs and their irregular, skew arrangement can be found in architecture in several projects [78–81], among others. However, SGPs have not yet been explored much as large-scale structures and architectural design applications, and besides kinetic art, the creative discipline of architecture can open new avenues by the paired aspects of functionality and aesthetics of the transformation of structures. In this regard, the 2-Landscapes pavilion [82] that explores the transformability of spaces

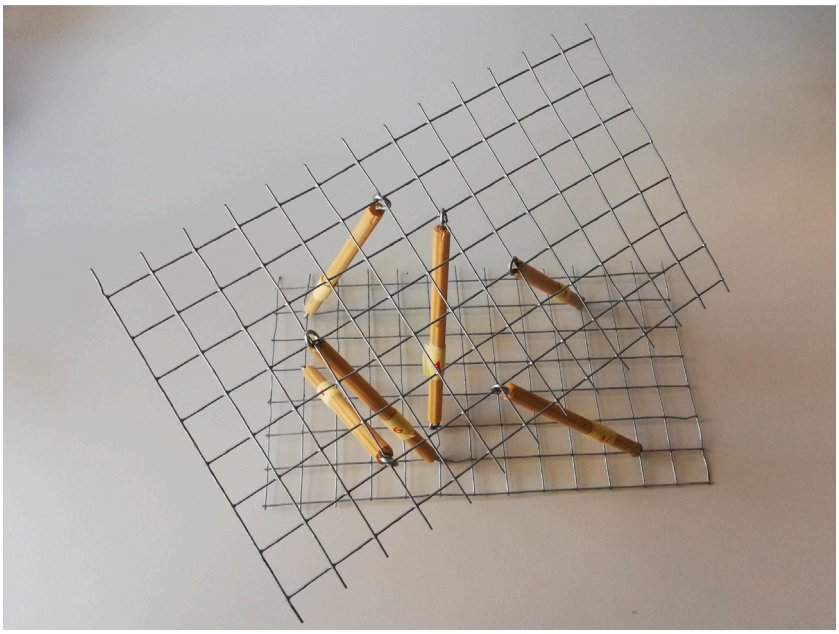

Fig. 3. A preliminary scaled model of the Zero Gravity project.

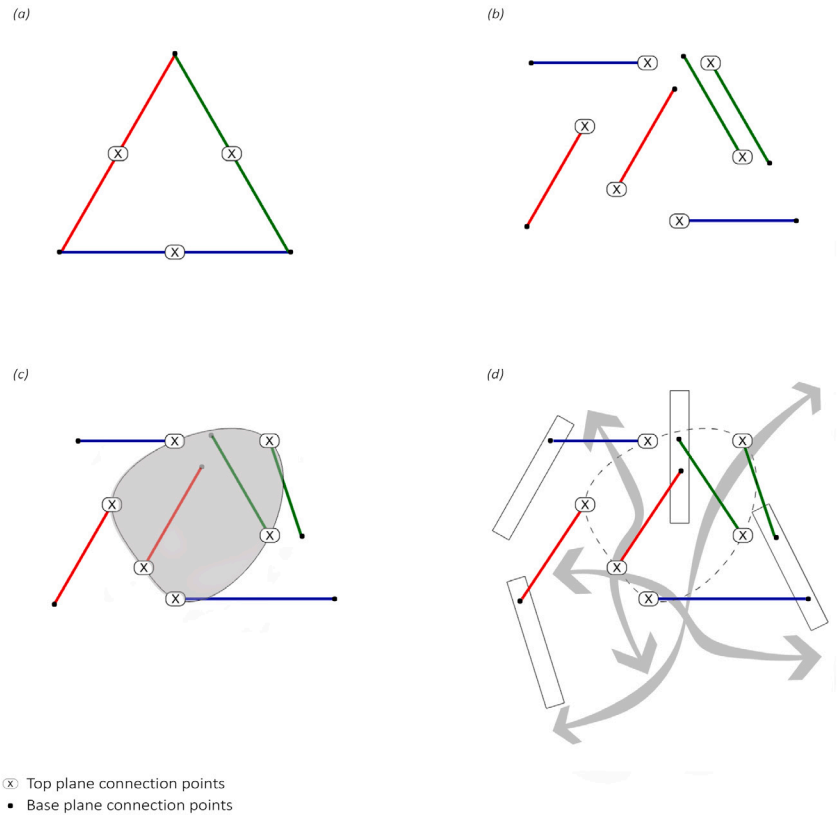

Fig. 4. Design and concept development of the Zero Gravity project in top view. A 3–3 configuration (a) from 3 pairs of legs arranged in an isosceles triangulated form being decomposed and rearranged to an irregular 6–6 configuration (b) by horizontal shifts of the 6 legs only. Marginal modifications (leg lengths, leg rotation) due to architectural and structural requirements such as nearly circular arrangement of the legs' top ends (c), resulting in a satisfying 6–6 starting configuration (pose) (d).

and the associate movement of the aluminum roof panels by combining two layers of elastic grid-shells by an irregular 6–6 SGP, is the only architectural structure of its kind known to the authors.

1.3. Goal and overview

Our research aims to explore SGP as an architectural object and its coalesce structural performance, unlocking its functional and aesthetic potentials for these disciplines accordingly. More specifically,

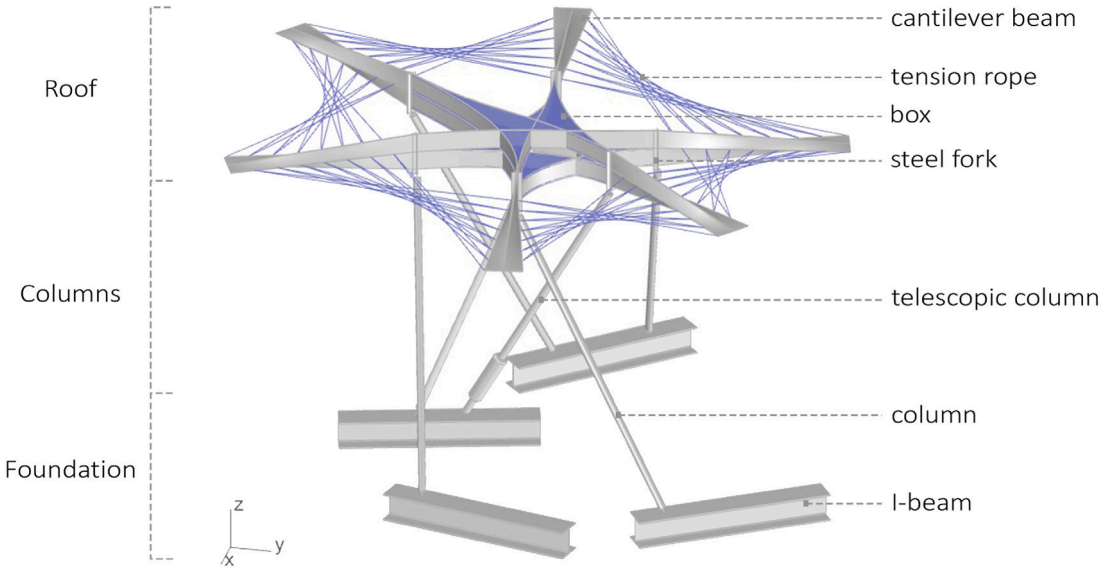

Fig. 5. Digital model of Zero Gravity structure.

we suggest a kinematic pavilion as an architectural object of a 6–6 SGP. Our study and realized pavilion is inspired by [82–85] and therefore considers the mechanism as an architectural object from both perspectives: (i) as a constantly transforming, architectural space and (ii) as a structural system with changing geometry.

We have provided a historical review of SGPs in a wide variety of fields and we have explored SPG as architectural object. In Section 2 the project of the kinematic pavilion is presented, while in Sections 3 and 4 , the equilibrium equations along with the kinematics of the system are explained. In Section 5, the driving factors of the design process towards the decision for the telescopic leg selection of the kinematic pavilion are presented in more detail. The final conclusions of the design study are presented in Section 6.

2. The Zero Gravity pavilion project

The Zero Gravity pavilion (Fig. 2), emerged from a design-build [86] and a multidisciplinary co-creation process [87,88], and serves as a showcase considering the realized SGP as an architectural object that is constantly transforming the architectural space. The transformation is initiated by a human-structure interaction, which changes the role of the visitor to the role of an actively influencing user. Simultaneously, the pavilion is a structural system with changing geometry, which is among other requirements a key aspect for the design process.

2.1. Concept and design

Elegantly moving structures seem to visually overcome gravity. Along these lines, the design process of the Zero Gravity pavilion was initiated by firstly exploring scaled, physical models as shown in Fig. 3, and later by the parallel use of computational models for architectural purposes and structural evaluation. Two major, cyclical design phases – (i) finding a 6–6 starting configuration (pose) and (ii) finding the most appropriate leg for being actuated for the specific pose – were made for finding a multiobjective solution, which is technically and structurally feasible, architecturally suitable and aesthetically pleasing. The predominantly considered parameters for our design phases encompass (i) structural considerations including the stability of the structure, the distribution of the roof's selfweight on a nearly circular arrangement of the legs' top ends, the force distribution and the change of forces during motion, the speed of the motion (dynamic effect) in dependence of distance of legs' top ends, collision of the structure and self-collision of legs, (ii) architectural requirements characterized by functional aspects including the visitor flow and place-making, the clearance below the roof and between the columns, the size of the realized structure, the magnitude (workspace) and speed of motion of the roof, the transition and inclination of columns, (iii) aesthetic aspects such as the generated architectural open space at the base plane, the type, path and speed of motion, the human-structure interaction by the sensor-activated motion of the pavilion, and (iv) economic aspects characterized by the general low-budget resulting in decisions such as having two legs on the same support (I-beam), one actuated leg only, which is easy to produce and to maintain, and the overall size of the realized pavilion.

In a first design phase, the Stewart–Gough 3–3 configuration (Fig. 4(a)) was rearranged to an irregular 6–6 configuration (Fig. 4(b)). The initial 3–3 design was assembled from 3 pairs of legs with equal lengths and inclination, thus forming a stable structure from isosceles triangles and providing a platform (roof) parallel to its base. Along above-mentioned architectural, aesthetic and economic parameters, the 3–3 SGP structure was stepwise decomposed and modified to a 6–6 configuration by horizontal shifts and neither changing the legs' lengths nor the direction vector of the legs. All these horizontal shifts do not create any motion on the platform or the base. This way, the changes in the leg arrangement resulted in a stable overall structure, which was checked mathematically by computing the determinant of the rigidity matrix. (see Appendix A). Contrary, this increased the architectural freedom in the arrangement of leg elements and design. The 6–6 configuration (pose) as illustrated in Fig. 4(b) was slightly modified (Fig. 4(c)) to meet requirements such as nearly circular arrangement of the legs' top ends or having two legs on the same support (I-beam). Finally, the legs' lengths were marginally adjusted and only one leg was slightly rotated for architectural reasons, resulting in a satisfying 6–6 starting configuration (pose) as shown in Fig. 4(d). Consequently, the structure was checked against stability and collision in the starting position and during motion.

Early in the design process, it was decided to opt for only one of the six articulated legs as a linear telescopic actuator for several reasons including the following main aspects:

(i) Due to clearance, a subject of safety, the roof was supposed to use a comparably limited workspace restricted to a linear actuation of +/− 0.50 m.

(ii) A 5+1-set-up of legs offers the possibility to separately investigate the motion of the platform depending on the actuated leg. Our selection

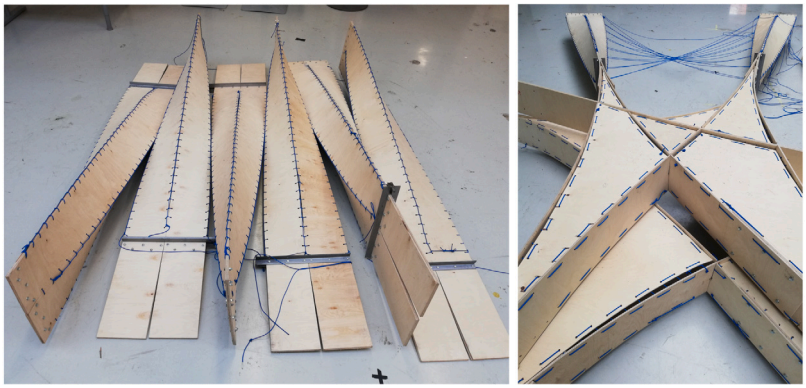

Fig. 6. Six cantilevers before assembly (left) and central grid structure of the roof (right).

Fig. 7. Spherical joint detail of column (left) and fork detail that connects the roof with the column of the pavilion (right).

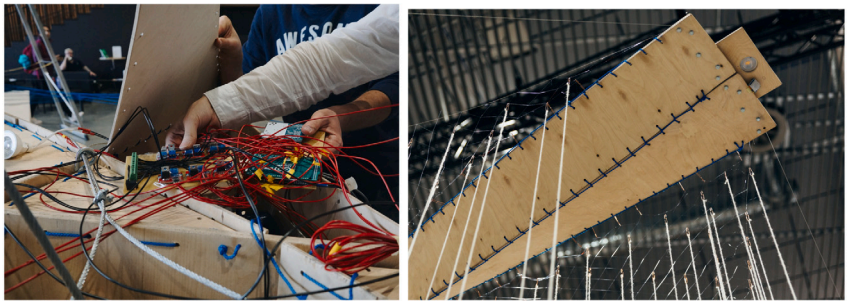

Fig. 8. Installation of Arduino controlled sensor (left) and spotlights at the tip of the roof's cantilevers (right).

of a specific actuated leg is based on structural consequences and architectural requirements, visually appealing motion and transformation, and structural performance as described in Sections 5 and 6.

(iii) Linearly actuated by one leg, limited in length change, the platform follows a certain path that is part of a curve with degree 20. In the realized structure, the constant back and forth motion of the roof is not perceived by the viewer as repetitive.

(iv) One linearly actuated leg asks for one single needed motor that can be located in any of the six legs. Compared to linearly actuated columns, fixed length columns are cheap and easy to produce and to maintain. This has a positive impact on the cost, weight, and design of the leg elements.

The question of self-collision like leg interference is of interest and an important aspect in the design of such a kinematic pavilion. Usually, it is the aim to find self-collision-free realizations over the complete motion cycle, which is quite a challenging task [71]. Even though there are many approaches for search strategies for finding a self-collision free setup, [76,89,90], the collision-avoidance of our structure is based on scaled physical models and on two separate computational models, see Section 5.

Even though this paper does not aim to provide a stepwise design procedure for other designers, altogether, the finally selected configuration resulted from an iterative exploration of the architectural and structural design space, as explained above. Most of the design-driving parameters can be rationalized, and their results can be compared and evaluated, supporting the decision-making process towards the final project. In addition, the design process also includes creative, intuitive and artistic aspects usually described in literature as the black box design process [91]. However, also the creative process of architectural design is usually considered cyclical and iterative [92], as it narrows down the possibilities until all architectural drivers have been addressed in the creative design process to a feasible and meaningful solution.

At this crossroad, the Zero Gravity kinematic pavilion [41], see Fig. 2, was designed, developed, built and exhibited by the multidisciplinary team of Aalto University Structures and Architecture at the Väre building, Aalto University, Espoo, Finland in 2019.

Fig. 9. Visualization of the transformable space of the Zero Gravity pavilion through suspended "hair" and the "falling leaves", (Photo credit: Lassi Savola).

2.2. Realization

The pavilion consists of three main parts, (i) a moving platform, namely the lightweight roof, (ii) six articulated columns, five of which with fixed lengths plus one linearly actuated column, and (iii) I-beams on the fixed base-plane (floor), serving as benches and as temporary heavy-weight foundations for the columns, Fig. 5.

For the realization of the full-scale structure we used thin 6.5 mm plywood for the central part of the roof with its cantilevering beams (Fig. 6) [93]. The lateral stability and rigidity of the cantilevering part of the roof was achieved by a triangulated rope pattern (Figs. 2, 5), later replaced by a net-structure, see Fig. 8 right. These modifications were done for exploring spatial qualities during motion, visualized by the suspended "hair" and the "falling leaves" Fig. 9, but their shape generation and artistic meaning are not within the scope of this paper. This way, the Zero Gravity pavilion covered an area of about 40m^2 with a total weight of 150 kg for the roof. Thin unprocessed birch-wood trees with a diameter of about 70 mm served as columns, see Fig. 7 left. Spherical joints were attached at both ends of the birch trunks, see Fig. 7 left, and the lightweight roof was connected to the columns by fork elements from steel, Fig. 7 right. One of the columns was executed as telescopic leg, by means of a servomotor-driven, metric screw. The screw provided the possibility to extend and to shorten the initial length of the column by 0.5 m, which represents a total change of length of 1 m. Metal connectors and spherical joints, see Fig. 7 right, were used for the manufacturing and the assembly process, which was supported by architecture and engineering students from Aalto University. Finally, the bottom ends of the columns were connected to steel I-beams, which functioned as both, the temporary heavy-weight foundation of the pavilion and as benches for the visitors.

2.3. Human-structure interaction

The motion of the structure allowed for an intended human-structure interaction of the Zero Gravity pavilion, by use of components from the Arduino open-source electronics platform [94], which controlled the sensors, the spotlights and the motor, which actuated the motion of the structure. The full cycle of motion was divided into six equal sequences, corresponding to the amount of cantilever beams of the roof. The sensors and spotlights were attached at each cantilever beam's free end (tip), see Fig. 8 right. When approaching the pavilion, the structure was standing still, but the visitor moreover the user found a randomly switched on spotlight. By stepping into the spotlight, the sensors recognized the user and actuated the first sequence of the structure's motion, but only if the user would stay within the range of the sensor. At the end of each sequence, the spotlight was switched off. The user could activate the next sequence of motion by stepping again into another randomly switched on spotlight and so forth. In this way, an either/or-process was initiated, which practically means that either the user or the structure would be in motion. Consequently, the user would explore the architectural space by moving through and around the structure, or the transformation of the space would be visible for the static user. The only way to by-pass the system and explore the transforming structure by simultaneously moving around it, is by working as a team of two or more users. However, the spotlights served as a guiding system, in the sense that after having activated all sensors and sequences by stepping into six consecutively switched on spotlights, the user has basically explored the space during a full cycle of motion from different viewpoints. The randomness in activated spotlights guaranteed that the user would experience different combinations of motions and standpoints, even after several visits.

Table 1
Number of nodes of column members n, where p denotes the base point of the column and $p+6$ the roof point, see Fig. 10.

Elements n		1	2	3	4	5	6
Nodes	p	1	2	3	4	5	6
	p + 6	7	8	9	10	11	12

3. Equilibrium equations

The system presented herein is a statically determinate system and therefore the six equations of equilibrium are enough to calculate the internal forces in each of the six columns by assuming that the roof behaves as a rigid body, Fig. 10, [95]. It should also be noted that the motion of the structure is very slow and therefore the behavior of the system is assumed as static.

A column element n in space is defined by points p and $p+6$, see Table 1 and Fig. 10, with unit vector $\vec{e}^{(n)}$, length vector $\vec{l}^{(n)}$, while its

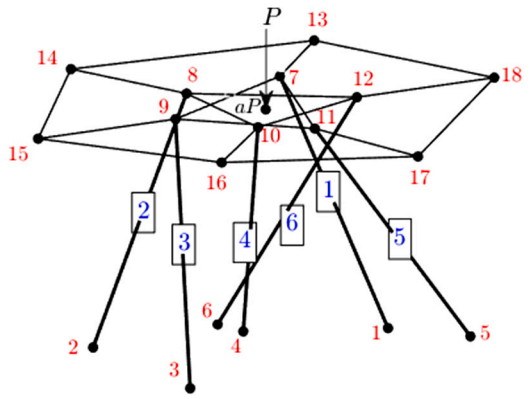

Fig. 10. Structural system of the Zero Gravity pavilion, numbers in squares (blue) denote leg elements/columns, the rest (red) denote nodes such as pin joints from the legs or free ends (tips) of the cantilever beams and point aP denotes the point of application of external load P.

length is $l^{(n)}$, see Fig. 11, Appendix A. The force vector $\vec{N}^{(n)}$ of element n shown in Fig. 11 can be written as:

$$\vec{N}^{(n)} = N^{(n)}\left(\frac{x_p^{(n)} - x_{p+6}^{(n)}}{l^{(n)}}\vec{i} + \frac{y_p^{(n)} - y_{p+6}^{(n)}}{l^{(n)}}\vec{j} + \frac{z_p^{(n)} - z_{p+6}^{(n)}}{l^{(n)}}\vec{k}\right) \tag{1}$$

where $N^{(n)}$ is the magnitude of internal axial force of element n. The equilibrium equations of all normal forces in x, y, z directions can be calculated as follows:

$$\sum F_x = 0 \Leftrightarrow \sum_{n=1}^{6} N^{(n)}\frac{x_p^{(n)} - x_{p+6}^{(n)}}{l^{(n)}} = 0 \tag{2}$$

$$\sum F_y = 0 \Leftrightarrow \sum_{n=1}^{6} N^{(n)}\frac{y_p^{(n)} - y_{p+6}^{(n)}}{l^{(n)}} = 0 \tag{3}$$

$$\sum F_z = 0 \Leftrightarrow \sum_{n=1}^{6} N^{(n)}\frac{z_p^{(n)} - z_{p+6}^{(n)}}{l^{(n)}} = P \tag{4}$$

where $P = 150$ kg is the resultant of the weight of the roof, which can be written in vector form as:

$$\vec{P} = 0\vec{i} + 0\vec{j} - P\vec{k} \tag{5}$$

The three additional equations are provided by the moments, which are calculated around point 7, namely top of column 1 see Fig. 10 by the following expression:

$$\vec{M}_{1n} = \vec{r}_{1n} \times \vec{N}^{(n)} \tag{6}$$

where $\vec{r}_{1n}$ is the position vector at the roof level and is defined by Eq. (A.4).

The equations of equilibrium regarding moments around axes x, y, z are calculated as follows:

$$\sum M_x = 0 \Leftrightarrow \sum_{n=1}^{6}\left[N^{(n)}\left((y_{p+6}^{(n)} - y_{p+6}^{(1)})\frac{z_p^{(n)} - z_{p+6}^{(n)}}{l^{(n)}} - (z_{p+6}^{(n)} - z_{p+6}^{(1)})\frac{y_p^{(n)} - y_{p+6}^{(n)}}{l^{(n)}}\right)\right] = -P\left((y_{p+6}^{(1)} - y_{p+6}^{(P)})\right) \tag{7}$$

$$\sum M_y = 0 \Leftrightarrow \sum_{n=1}^{6}\left[N^{(n)}\left((z_{p+6}^{(n)} - z_{p+6}^{(1)})\frac{x_p^{(n)} - x_{p+6}^{(n)}}{l^{(n)}} - (x_{p+6}^{(n)} - x_{p+6}^{(1)})\frac{z_p^{(n)} - z_{p+6}^{(n)}}{l^{(n)}}\right)\right] = -P\left((x_{p+6}^{(P)} - x_{p+6}^{(1)})\right) \tag{8}$$

$$\sum M_z = 0 \Leftrightarrow \sum_{n=1}^{6}\left[N^{(n)}\left((x_{p+6}^{(n)} - x_{p+6}^{(1)})\frac{y_p^{(n)} - y_{p+6}^{(n)}}{l^{(n)}} - (y_{p+6}^{(n)} - y_{p+6}^{(1)})\frac{x_p^{(n)} - x_{p+6}^{(n)}}{l^{(n)}}\right)\right] = 0 \tag{9}$$

The equilibrium equations are written in matrix form:

$$\mathbf{F} = \mathbf{A}\mathbf{X} \tag{10}$$

where $\mathbf{F}, \mathbf{A}, \mathbf{X}$ are defined in Appendix A. The system is solved with the *linsolve* function in MatLab:

$$\mathbf{X} = \mathbf{A}^{-1}\mathbf{F} \tag{11}$$

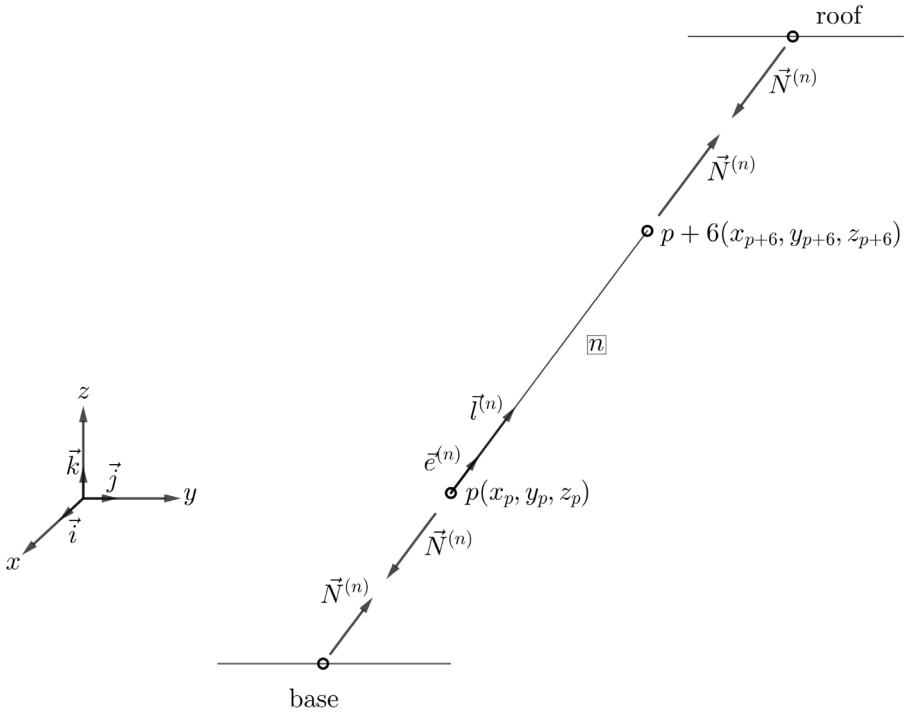

Fig. 11. An element n in space.

The system of Eq. (11) is linear and has unique solution when the determinant of the rigidity matrix **A** is different from zero, $det(\mathbf{A}) \neq 0$.

4. Kinematics

In this section the kinematics of the SGP are solved. As stated by Husty [42], when only six distance measurements are available, the direct kinematic problem of parallel manipulators has forty solutions, some of which might be complex. Therefore, when solving the direct kinematics of SGP, a process that defines the unique solution of the platform configuration, should be followed. Along these lines in the current study, scaled models along with computational models have been used to define the starting configuration (pose) of the platform parallel to the base. As a first step, by using the inverse kinematics the leg lengths of the pavilion at the starting pose are defined. In the next step, only one length of the pavilion's legs changes very slightly, while the rest of the legs have constant length. In this way, the pose of the platform will not change drastically. Therefore, the so-called nearby pose of the platform is derived. Thus, we have a starting value when trying to solve numerically the new position of the platform. Consequently, we obtain the unique solution of the direct kinematics of the platform (as far as the determinant of matrix **A** is different from zero). All further changes of the leg length use the previous pose of the platform as a starting value of the numerical solution process. The computation of the determinant of matrix **A**, the Jacobian matrix, has shown that none of the computed poses is close to a singularity (determinant of **A** is equal to zero), which means that no other solution of the direct kinematics is close to the obtained pose of the platform.

To solve this pose problem the approach presented in [42] in a slightly modified version is applied. In this approach, the displacement matrix is parametrized using Study coordinates. First of all two coordinate systems are attached to the roof (O_m, x_m, y_m, z_m) and the base (O_f, x_f, y_f, z_f) of the pavilion model. The coordinates of all points (base and roof points of the columns) in the base coordinate system are presented in Table 2. Additionally, the initial coordinates of the tips of the cantilevers are presented in Table 3 in the base coordinate system. The origin of the moving (roof) coordinate system lies at point (0,0,3) of the base coordinate system. The transformation matrix **T** between the moving and the fixed coordinate system in homogeneous Study coordinates is:

$$\mathbf{T} = \frac{1}{\Delta}\begin{bmatrix} \Delta & 0 & 0 & 0 \\ u & x_0^2+x_1^2-x_2^2-x_3^2 & 2(x_1x_2-x_0x_3) & 2(x_1x_3+x_0x_2) \\ v & 2(x_1x_2+x_0x_3) & x_0^2-x_1^2+x_2^2-x_3^2 & 2(x_2x_3-x_0x_1) \\ w & 2(x_1x_3-x_0x_2) & 2(x_2x_3+x_0x_1) & x_0^2-x_1^2-x_2^2+x_3^2 \end{bmatrix} \tag{12}$$

$$\begin{aligned} u &= 2(-x_0y_1 + x_1y_0 - x_2y_3 + x_3y_2), \\ v &= 2(-x_0y_2 + x_1y_3 + x_2y_0 - x_3y_1), \\ w &= 2(-x_0y_3 - x_1y_2 + x_2y_1 + x_3y_0), \\ \Delta &= x_0^2 + x_1^2 + x_2^2 + x_3^2 \end{aligned} \tag{13}$$

The eight coordinates are homogeneous and linked by the so called Study equation:

$$S: \quad x_0y_0 + x_1y_1 + x_2y_2 + x_3y_3 = 0, \qquad x_i \quad \text{not all} \quad 0 \tag{14}$$

Following [42] the six distance equations can be written

$$(Q_n - Q_{n+6})^T(Q_n - Q_{n+6}) - (l^{(n)})^2 = 0, \quad n = 1, 2, \dots, 6 \tag{15}$$

where Q_n are the coordinates of the base attachment points of the legs (nodes $1, \dots, 6$ in Table 2). The coordinates Q_{n+6} can be computed from

$$Q_{n+6} = \mathbf{T}q_{n+6}, \quad n = 1, 2, \dots, 6 \tag{16}$$

Table 2
Initial coordinates of top and base points of column members (Fig. 10) in the base coordinate system (O_f, x_f, y_f, z_f).

Elements	Nodes Q	x (m)	y (m)	z (m)
1	1	5.5	3.5	0
	7	5	5	3
2	2	2	5	0
	8	3.5	5	3
3	3	1.5	2.5	0
	9	2.5	4	3
4	4	4	4.5	0
	10	3	3	3
5	5	6	2.5	0
	11	3.5	2.5	3
6	6	4	5	0
	12	5	3.5	3

where q_{n+6} are the coordinates of the moving nodes in the moving coordinate system (x,y coordinates of nodes $7, \dots, 12$ in Table 2). Eqs. (15) are quartic equations in Study coordinates $(x_i, y_i, i = 0, \dots, 3)$, but can be reduced without loss of generality [42] to quadratic equations by adding $4S^2$.

$$h_n: \ (Q_n - Q_{n+6})^T(Q_n - Q_{n+6}) - (l^{(n)})^2 + 4S^2 = 0, \quad n = 1, 2, \dots, 6 \tag{17}$$

where $l^{(n)}$ can be computed from Q_n and Q_{n+6} from Table 2 and this yields

$$l^{(1)} = \frac{\sqrt{46}}{2}, l^{(2)} = \frac{3\sqrt{5}}{2}, l^{(3)} = \frac{7}{2}, l^{(4)} = \frac{7}{2} + t, l^{(5)} = \frac{\sqrt{61}}{2}, l^{(6)} = \frac{7}{2} \tag{18}$$

In this case, $l^{(4)}$ is the leg which will be the telescopic one and therefore, a parameter t is added to its length. When other legs will be the telescopic ones, the parameter t will be added to their length. To solve the pose problem a set f of eight equations is produced from Eqs. (17) and S as follows:

$$\begin{aligned} f = [&x_0 = 1, h_1, h_2 - h_1, h_3 - h_1, h_4 - h_1, h_5 - h_1, h_6 - h_1, S] \Rightarrow \\ f = [&x_0 - 1, -9x_0^2 + 40x_0x_3 + 2x_0y_1 - 6x_0y_2 + 61x_1^2 - 180x_1x_2 \\ &- 2x_1y_0 - 34x_1y_3 + 101x_2^2 + 6x_2y_0 + 42x_2y_3 + 171x_3^2 + 34x_3y_1 \\ &- 42x_3y_2 + 4y_0^2 + 4y_1^2 + 4y_2^2 + 4y_3^2, \\ &- 70x_0x_3 - 8x_0y_1 + 6x_0y_2 + 30x_1^2 + 70x_1x_2 + 8x_1y_0 - 6x_1y_3 \\ &- 82x_2^2 - 6x_2y_0 - 20x_2y_3 - 52x_3^2 + 6x_3y_1 + 20x_3y_2, \\ &- 41x_0x_3 - 6x_0y_1 - 30x_1^2 + 131x_1x_2 + 6x_1y_0 + 8x_1y_3 - 95x_2^2 \\ &- 26x_2y_3 - 125x_3^2 - 8x_3y_1 + 26x_3y_2, \\ &2x_0y_1 - 2x_1y_0 - 14x_2y_3 + 14x_3y_2 + \frac{49x_0^2}{4} - \frac{15x_1^2}{4} - \frac{199x_2^2}{4} \\ &- \frac{263x_3^2}{4} - \left(\frac{7}{2}+t\right)^2 x_0^2 - \left(\frac{7}{2}+t\right)^2 x_1^2 - \left(\frac{7}{2}+t\right)^2 x_2^2 - \left(\frac{7}{2}+t\right)^2 x_3^2 \\ &+ 12x_0y_2 + 4x_1y_3 - 12x_2y_0 - 4x_3y_1 - 46x_0x_3 + 78x_1x_2, \\ &- 15x_0x_3 + 8x_0y_1 + 6x_0y_2 - 45x_1^2 + 85x_1x_2 - 8x_1y_0 + 14x_1y_3 \\ &- 26x_2^2 - 6x_2y_0 - 4x_2y_3 - 71x_3^2 - 14x_3y_1 + 4x_3y_2, \\ &- 84x_0x_3 - 6x_0y_1 + 12x_0y_2 + 24x_1x_2 + 6x_1y_0 - 30x_2^2 - 12x_2y_0 \\ &- 6x_2y_3 - 30x_3^2 + 6x_3y_2, x_0y_0 + x_1y_1 + x_2y_2 + x_3y_3] \end{aligned} \tag{19}$$

The parameter x_0 can be set $x_0 = 1$ without loss of generality because the Study coordinates are homogeneous and $x_0 = 0$ would lead to an upside down assembly of the framework which is definitely not wanted for the architectural purpose. This system of equations completely solves the pose problem of the mechanical system. Especially it would allow to compute all the assembly modes. In the case of the pavilion this is not necessary. First of all it is easy to see that the numerical solution of f for the starting pose $t = 0$ is obtained by

$$x_0 = 1, x_1 = 0, x_2 = 0, x_3 = 0, y_0 = 0, y_1 = 0, y_2 = 0, y_3 = -1.5 \tag{20}$$

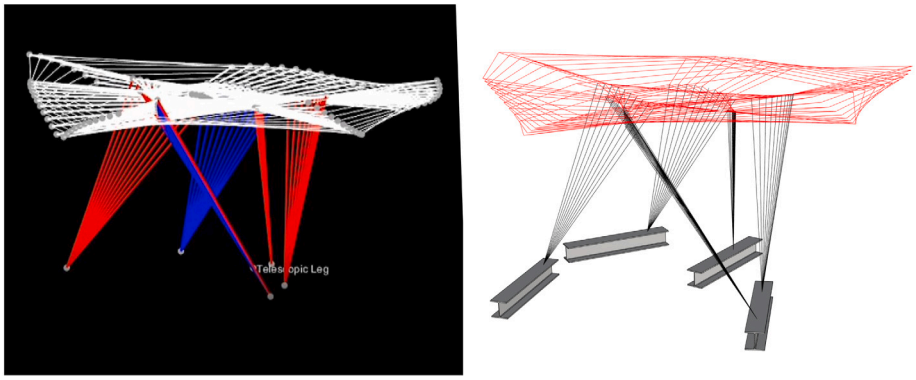

Fig. 12. Validation of the kinematics by the numerical model developed in MatLab through the one developed in Rhinoceros/Grasshopper.

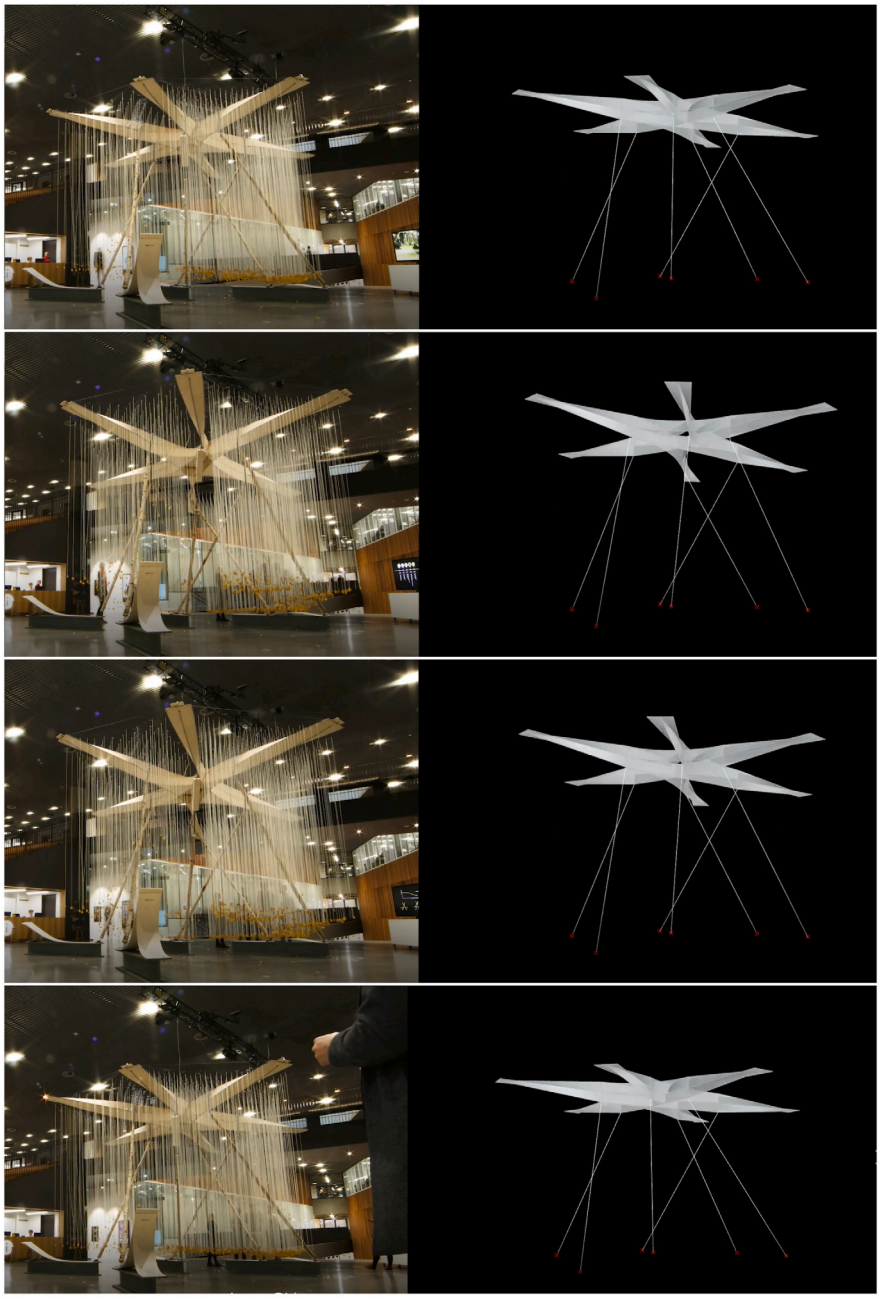

Fig. 13. Validation of the kinematics by the Zero Gravity pavilion of the numerical model in Rhinoceros/Grasshopper.

Table 3
Initial coordinates of cantilever members and point of application of the external load aP, see Fig. 10.

Nodes	x (m)	y (m)	z (m)
13	6.58	6.25	3
14	3.25	6.95	3
15	0.50	4.25	3
16	1.42	1.79	3
17	3.51	0.50	3
18	7.00	3.25	3
aP	3.70	3.70	3

which results in the transformation matrix

$$\mathbf{T}_0 = \begin{bmatrix} 1 & 0 & 0 & 0 \\ 0 & 1 & 0 & 0 \\ 0 & 0 & 1 & 0 \\ 3 & 0 & 0 & 1 \end{bmatrix} \tag{21}$$

Substituting e.g. $t = 0.05$ into the system f and numerically solving with the starting value $x_0 = 1, x_1 = 0, x_2 = 0, x_3 = 0, y_0 = 0, y_1 = 0, y_2 = 0, y_3 = -1.5$ yields

$$\begin{aligned} &x_0 = 1.000000000, x_1 = -0.001669497310, x_2 = 0.008559319407, \\ &x_3 = 0.01475519880, \\ &y_0 = 0.02211326466, y_1 = -0.04031998574, y_2 = 0.07689857451, \\ &y_3 = -1.547846189 \end{aligned} \tag{22}$$

with the transformation matrix

$$\mathbf{T}_1 = \begin{bmatrix} 1 & 0 & 0 & 0 \\ 0.1093003542 & 0.9994182153 & -0.02953030215 & 0.01706435837 \\ -0.1470173026 & 0.02947315990 & 0.9995591233 & 0.003590528767 \\ 3.095002287 & -0.01716286449 & -0.003085499289 & 0.9998479467 \end{bmatrix} \tag{23}$$

and the position of the first node can be computed via

$$\mathbf{T}_1 \begin{pmatrix} 1 \\ q_{17} \\ q_{27} \\ q_{37} \end{pmatrix} = \begin{bmatrix} 1.0 \\ 4.958739919949999930 \\ 4.99814411339999953 \\ 2.99376046810499963 \end{bmatrix} \tag{24}$$

where q_{17}, q_{27}, q_{37} represent the moving coordinates, x, y and z respectively, of point 7 in the moving coordinate system. Similar computation for the other nodes yields their coordinates in the base frame and it can be easily checked that the leg length constraint is fulfilled for all of them. Using these coordinates the determinant of the stiffness matrix **A** can be computed which is far from zero for all values of t and therefore all these poses are stable configurations of the framework.

The problem of kinematics was solved in MatLab, [96]. Additionally, a geometric model was developed in Rhinoceros/Grasshopper environment, [97]. The comparison of the kinematics between the model developed in MatLab and the one developed in Rhinoceros/Grasshopper, is shown in Fig. 12, which clearly demonstrates that the two models provide identical results. Finally, the validity of the current approach is proven by the comparison of the kinematics of the Rhinoceros/Grasshopper model with the Zero Gravity pavilion, shown in Fig. 13 at different time instances.

5. Kinematic pavilion application

In this chapter we investigate the behavior of the Zero Gravity system in order to establish the choice of the telescopic leg based upon four criteria: stability range, self-collision and leg interference, force distribution and path trajectory.

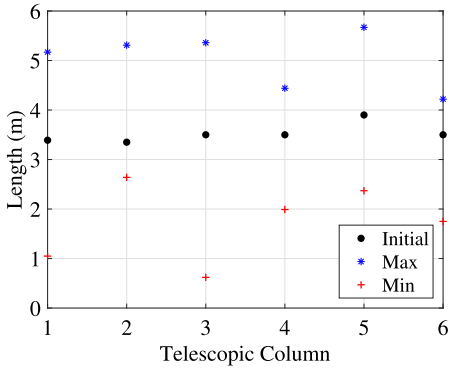

Fig. 14. Stability range of each telescopic column.

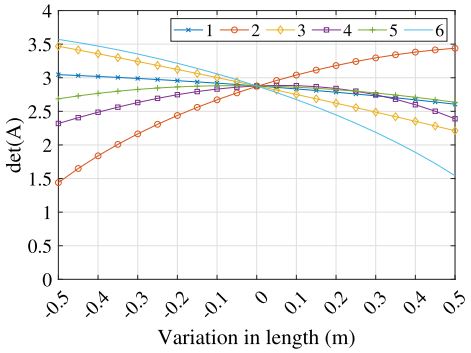

Fig. 15. Variation of determinant of matrix **A** for each telescopic leg.

5.1. Stability range

In order to investigate the stability of the SGP, the behavior of matrix **A** of Eq. (11) is checked. If the determinant of matrix **A** is equal to zero, it follows that the system is not stable and behaves as a mechanism. On the other hand, if the determinant of matrix **A** is different than zero, then the system has only one solution and it is stable. According to that, Fig. 14 shows the stability range of the six telescopic columns individually, see also Table 4. More precisely, columns 2 and 6 have the shortest allowable length variation among the six columns, respectively −0.71 m and +0.72 m. Columns 1 and 5 have nearly symmetric span for elongation and shortening. More specifically, for column 1 the span is between +1.78 m and −2.24 m and for column 5 the span is between +1.77 m and −1.53 m. The ratio between the length elongation and the shortening is approximately equal to two thirds for columns 3 and 4. For column 4 the maximum length elongation is +0.94 m, while for column 3 it is equal to +1.86 m. Due to construction restrictions and in order to have all columns as a candidate option we limit our study to the length variation range between +0.50 m and −0.50 m.

Figure 15 shows the variation of the determinant of matrix **A** for each telescopic column. The largest variation of $det(\mathbf{A})$ occurs in columns 2 and 6. Additionally, as shown in Fig. 15 column 2 has a clear trend to instability through shortening, and column 6 through elongation. Columns 4 and 5 indicate a nearly symmetrical transition of $det(\mathbf{A})$, which is a sign of balanced behavior. Finally, columns 1 and 3 show a trend to instability through elongation.

5.2. Self-collision and leg interference

Due to the above-described restricted length variation of the linear actuation and limited workspace consequently, self-collision and leg interference could easily be checked by moving our scaled physical

Table 4
Stability range of telescopic column members.

Columns	1	2	3	4	5	6
Max length (m)	5.17	5.31	5.36	4.44	5.67	4.22
Initial length (m)	3.39	3.35	3.50	3.50	3.90	3.50
Min length (m)	1.05	2.64	0.62	1.99	2.37	1.75

Table 5
Extrema forces in P for each column for each telescopic column case.

Telescopic columns		1	2	3	4	5	6
1	max	−0.24	−0.22	−0.21	−0.24	−0.24	−0.26
	min	−0.31	−0.34	−0.32	−0.30	−0.30	−0.28
2	max	0.23	0.26	0.36	0.24	0.30	0.16
	min	0.08	−0.29	−0.26	0.11	−0.03	−0.09
3	max	−0.34	0.07	0.11	−0.36	−0.20	−0.12
	min	−0.46	−0.61	−0.71	−0.51	−0.64	−0.49
4	max	−0.38	−0.36	−0.36	−0.21	−0.33	−0.37
	min	−0.44	−0.51	−0.57	−0.52	−0.51	−0.44
5	max	0.08	0.16	0.24	0.12	0.37	0.16
	min	0.03	−0.20	−0.17	−0.03	−0.19	−0.19
6	max	−0.27	0.01	−0.02	−0.27	−0.11	−0.04
	min	−0.28	−0.28	−0.34	−0.32	−0.42	−0.32

models [71]. Furthermore, A parametric and kinematic 3d-model was set up in the Rhinoceros/Grasshopper environment [98], which included all real dimensions and geometries (profiles) of the elements of the later realized structure, and which served for the architectural design. The later realized path of the platform and the motion of the columns were subdivided by splitting the 1 m range of the actuated column into 0.1m-steps. The closest points between the individual columns, as well as the distance between the roof and the columns were observed visually by the computational analysis. Additionally, a computational model set up in Matlab [96], provided a numerical analysis over the motion cycle of the structure. Like in the parametric model, the motion was split into small steps and the geometry was checked against collision accordingly.

5.3. Force distribution

During the length variation of the telescopic columns, the change of force distribution for each column is investigated. The results are presented in Fig. 16 and Table 5. In the case of telescopic column 1, the force variation of all columns is almost constant. The largest variation occurs in column 2, while column 5 is almost unloaded, Fig. 16(a). In the case of telescopic column 2, a wider range of force variation is observed, Fig. 16(b). More specifically, in column 3 a force variation of $0.68P$ occurs, while in column 2 the range is equal to $0.55P$ with load reversal from compression to tension. In addition to column 2, a load reversal occurs in columns 3, 5 and 6. In the case of telescopic column 3, the largest force variation occurs in column 3 itself and is equal to $0.82P$, Fig. 16(c). In columns 2, 3 and 5 load reversals from compression to tension can be observed. In the case of telescopic column 4, the largest load variation occurs in column 4 itself and is equal to $0.31P$, Fig. 16(d). In column 5, load reversal occurs from compression to tension. In case of telescopic column 5, the largest load variation occurs in column 5 itself and is equal to $0.56P$, Fig. 16(e). Additionally, columns 2 and 5 exhibit load reversal. In the case of telescopic column 6, the largest load variation occurs in column 3 and it is equal to $0.37P$, while load reversal occurs in columns 2 and 5, Fig. 16(e). Due to the fact that the roof of the structure is lightweight, the buckling of the columns was not considered.

Table 6
Clearance of the system for each telescopic column by adding the 30 cm of the I-beams where the columns are attached.

Columns	1	2	3	4	5	6
Clearance (m)	2.78	1.71	2.01	2.43	2.74	2.23

5.4. Path of kinematic structure

The path of the motion of the SGP was validated by using different computational tools, namely MatLab [96] with the method described in previous sections. Additionally, Rhinoceros/Grasshopper [97] with Kangaroo plug-in [99] within the Rhinoceros environment [98] was used. The results of the path trajectory are presented in Figs. 17, 18, 19, 20, 21, 22, where the elongation step for all figures is 20 cm. Apart from the path trajectory, the distance between the lowest point of the roof and the virtual top-plane of all I-beams, namely the clearance, is investigated, see Table 6. The clearance shown in Table 6 accounts also for the height of the I-beams (30 cm), which act as foundation of the pavilion. This way, the project provided enough clearance for the visitors on the ground plane and even when standing on the I-beams. Telescopic columns 2 and 3 exhibit clearance of 1.71 m and 2.01 m, which is not acceptable. Columns 1 and 5 exhibit dominant rotational motion, while column 6 exhibits dominant translational motion along the vertical axis. In column 4, both rotational and translational motion along the vertical axis can be observed. This type of motion is more observable to the visitors of the pavilion, taking into consideration that the motion of the structure is very slow in order to reduce the dynamic effects and to increase the visitor's experience.

5.5. Selection of telescopic leg

The selection of the telescopic leg of the pavilion is based on the four aforementioned criteria. More specifically, the stability range criterion investigated the stability of the global, structural system of the SGP, depending on the length variations of the six telescopic legs, but separately for each of them. In addition to clearance issues (safety) and due to construction limitations (length of used screw) the length variation of each column was restricted to ± 0.50 m. Leg interference and self-collision was thoroughly checked through the computational and physical models for each case separately. All telescopic columns were providing stable configurations within these limits, with columns 2 and 6 having the bounds closest to the limit. Columns 2 and 3 were excluded due to the insufficient clearance, see Table 6. Additionally, columns 2, 3 but also 5 were excluded due to undesirable load reversal. The load range distribution of column 5 is 0.56 P and it is larger compared to column 1 (0.15 P), column 4 (0.31 P) and 6 (0.37P). Therefore, the choice was to be made between columns 1, 4 and 6. The advantage of column 4 compared to columns 1 and 6 is that the motion is more expressive/visible and not limited as in the case of column 1. More specifically, the path trajectory of telescopic column 4 involves a balanced motion between rotational and translational movement around the vertical axis, compared to telescopic column 1, where the rotational component is dominant and to the telescopic column 6, where the translational movement is dominant. In the variation of force distribution in telescopic column 1, column 5 is almost unloaded, while in case of telescopic column 4, the force variation of column 5 is 3 times larger. Finally, due to the above-mentioned reasons, the telescopic column 4 was selected in the Zero Gravity pavilion realization.

6. Conclusions

In the current study, an SGP application of a kinematic pavilion is presented. After reviewing a wide range of SGP applications in various fields, SGP as an architectural object is explored (Section 1). The Zero Gravity structure was built in Espoo, Finland and its design

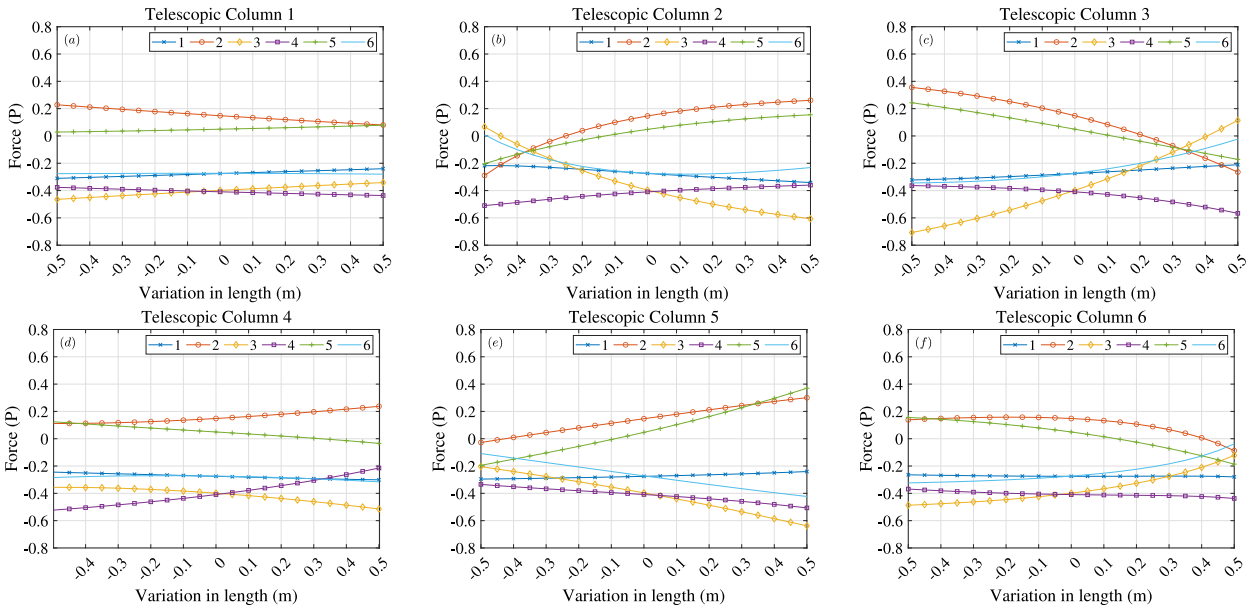

Fig. 16. Force distribution for telescopic column (a) 1, (b) 2, (c) 3, (d) 4, (e) 5 and (f) 6.

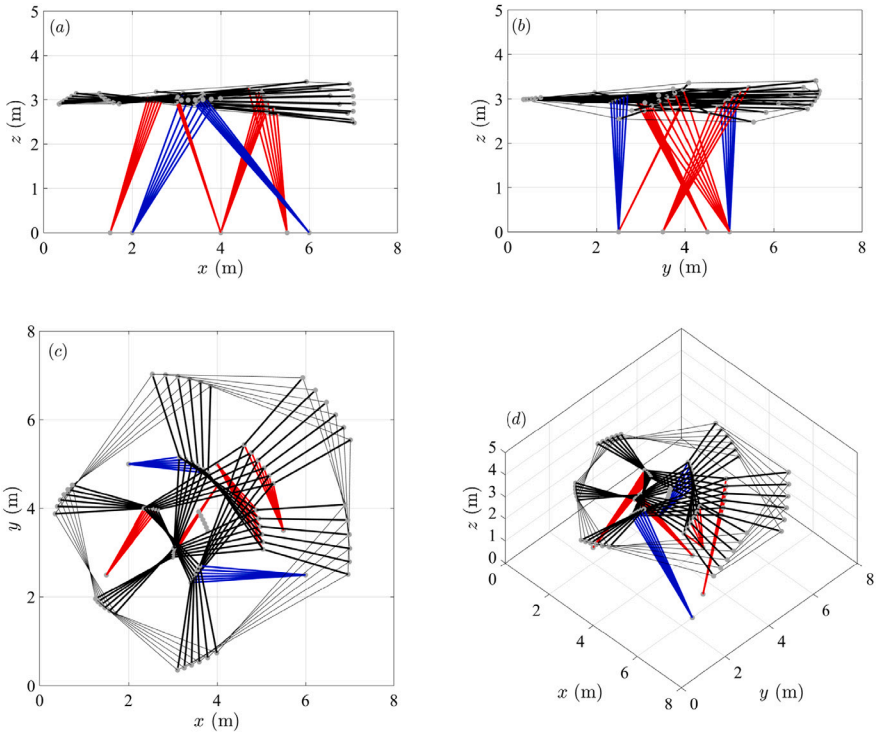

Fig. 17. Path of telescopic column 1: (a) X–Z plane, (b) Y–Z plane, (c) X–Y plane, (d) 3D.

and fabrication processes are explained (Section 2) along their decision making criteria (Section 5), which are of architectural, functional and structural nature, after establishing the equilibrium equations (Section 3) and the kinematics (Section 4). More specifically, the presented case study is based on an irregular, 6–6 configuration derived from the Stewart–Gough 3–3 configuration. In this sense, the Zero Gravity pavilion represents one of many initially feasible options. Its irregularity is rooted in architectural decisions, whereas the increased freedom in arrangement of columns is used for the functionality including visitor flows and place-making, and it is accompanied by structural stability and strength. Together with the decision for having only one linearly actuated leg these aspects come at the expense of the maximum workspace of the structure. But contrary to an SGP that adjusts all legs simultaneously (parallel manipulator), the Zero Gravity pavilion demonstrates an increased freedom in architectural design paired with a reduction in self-weight and costs, for the fabrication, installation and maintenance of the leg elements. Technically, configurations like the Zero Gravity pavilion set-up result in a complex sequence of translation and rotation on their paths, but with reduced elaborate programming and system-control. The visually appealing motion of the roof and the

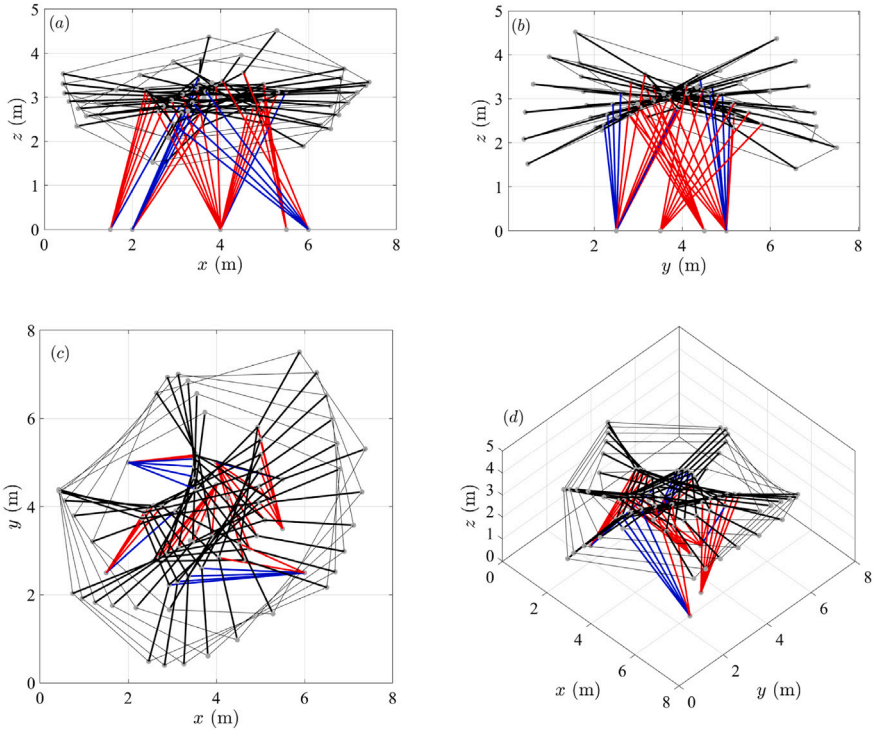

Fig. 18. Path of telescopic column 2: (a) X–Z plane, (b) Y–Z plane, (c) X–Y plane, (d) 3D.

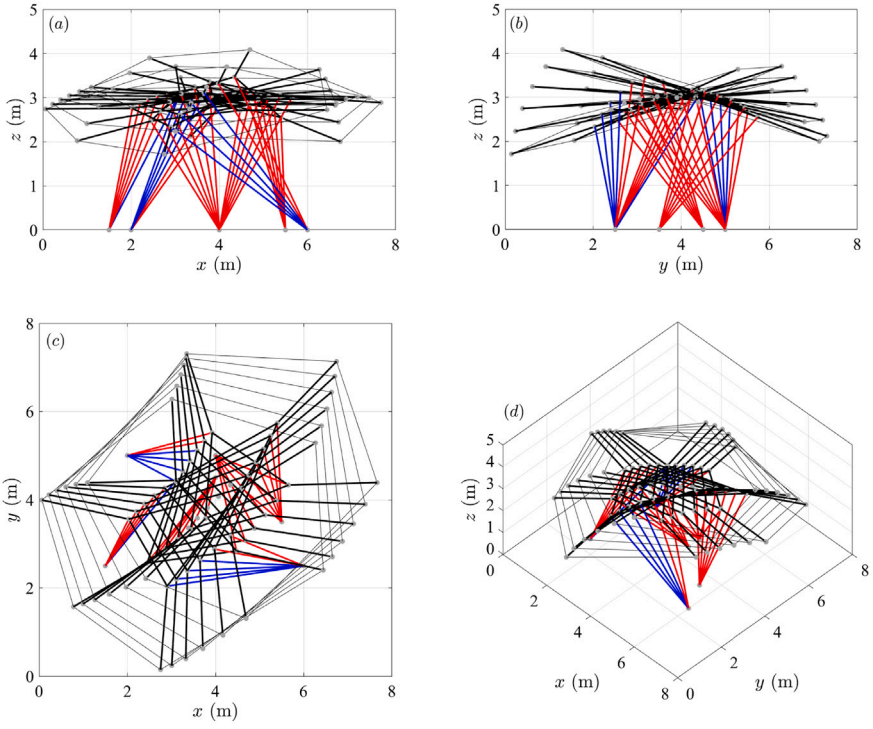

Fig. 19. Path of telescopic column 3: (a) X–Z plane, (b) Y–Z plane, (c) X–Y plane, (d) 3D.

inspiring, transforming architectural space emerged as a result from the described design of leg arrangement and the selection of the actuated leg 4. Through the human-structure interaction feature of the pavilion (Section 2.3), the user influences and experiences the pavilion's motion, which provides seemingly random and non-repetitive changes of the structure and architectural space.

To present, the general formulation of SGP has been mostly used as a theoretical model for mathematical and geometrical description, but has not been instrumentalized much in an applied sense in architecture. By applying it in an architectural scale, where the precision of SGP is not the primary goal, but at the same time other parameters are also focused on and new application possibilities can be opened up. Furthermore, SGP principles can help develop the built environment

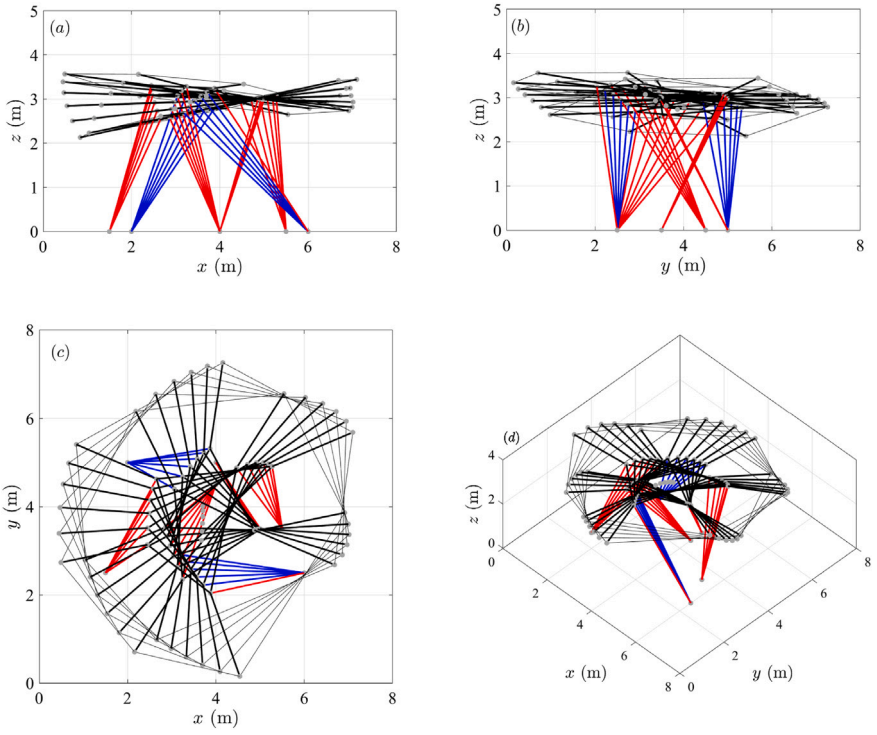

Fig. 20. Path of telescopic column 4: (a) X–Z plane, (b) Y–Z plane, (c) X–Y plane, (d) 3D.

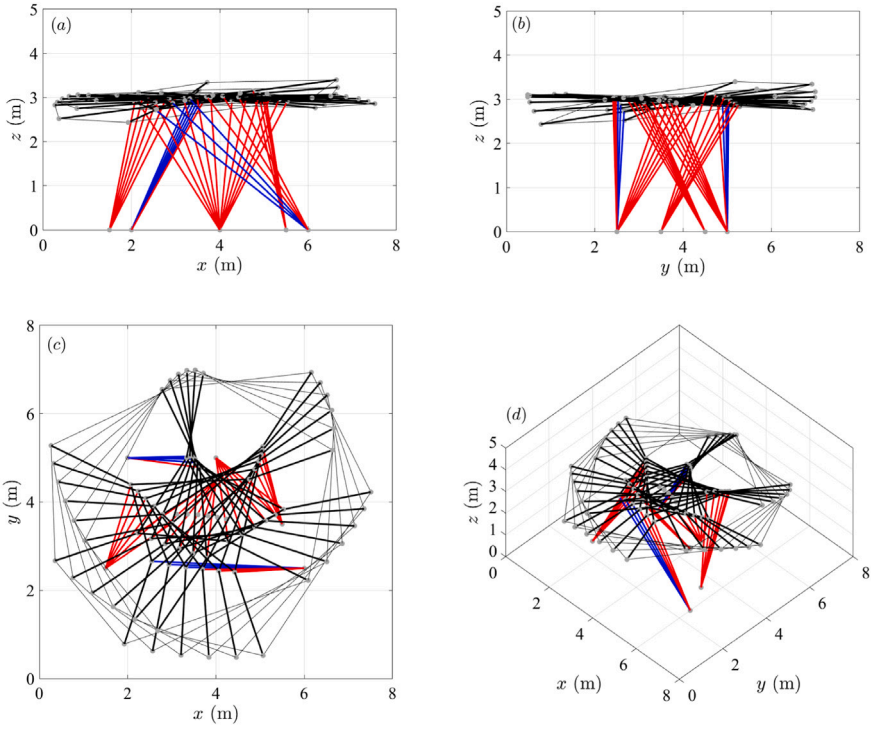

Fig. 21. Path of telescopic column 5: (a) X–Z plane, (b) Y–Z plane, (c) X–Y plane, (d) 3D.

from static to mobile, flexible, adaptable and transformable structures and architectures including change of position, volume and adaptability of inhabitable spaces. In addition, sustainability aspects like heating, cooling, ventilation, light supply, space consumption will benefit from this approach, which are subject of our ongoing research.

Finally, it is worth highlighting that the Zero Gravity pavilion contributes to the field of experimental and innovative architecture from several perspectives. The project emerged from a design-build process and a multidisciplinary co-creation setting in all stages from conceptual design to realization [100,101]. Therefore, the architectural space and spatial experience was iteratively shaped by a creative team of structural engineers, mechanical engineers, and architects [86,88,102,103]. The main contribution for architecture is seen in the shift of the SGP from a mechanism that facilitates motion, to a mechanism that

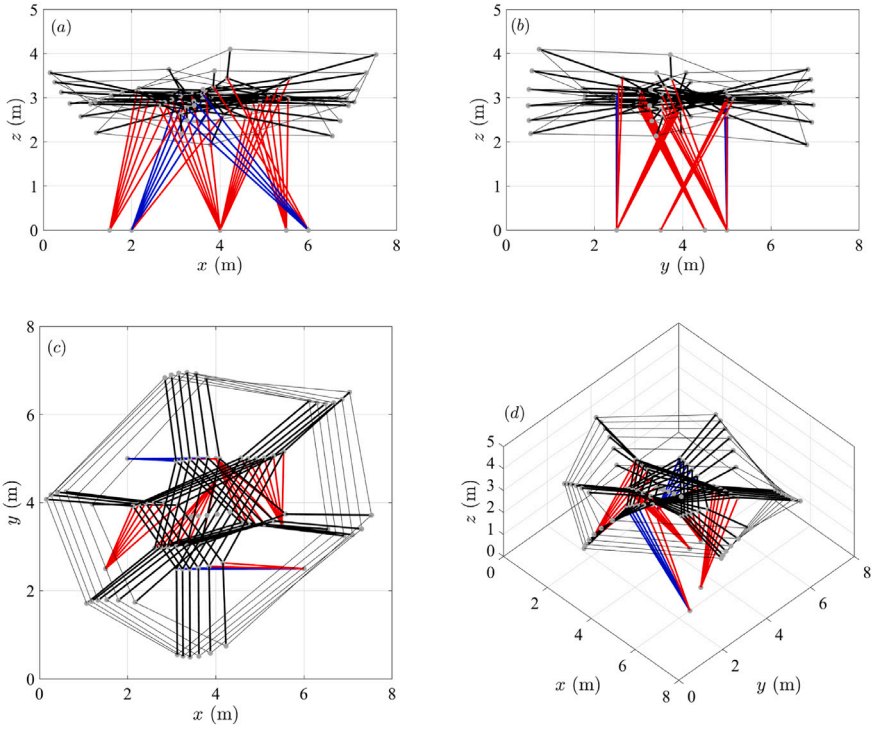

Fig. 22. Path of telescopic column 6: (a) X–Z plane, (b) Y–Z plane, (c) X–Y plane, (d) 3D.

serves as an architectural object and space. In this context, the essential feature of the architecture is the constantly transforming space, which is initiated by a human-structure interaction, changing the role of the visitor of the pavilion to the role of an actively influencing user.

CRediT authorship contribution statement

Athanasios A. Markou: Conceptualization, Methodology, Software, Supervision, Writing – original draft, Writing – review & editing, Data curation, Formal analysis, Investigation, Visualization. **Serenay Elmas:** Conceptualization, Methodology, Software, Visualization, Data curation, Investigation, Writing – original draft, Formal analysis, Validation. **Günther H. Filz:** Conceptualization, Methodology, Investigation, Resources, Writing – original draft, Writing – review & editing, Supervision, Funding acquisition.

Declaration of competing interest

The authors declare that they have no known competing financial interests or personal relationships that could have appeared to influence the work reported in this paper.

Acknowledgment

The authors would like to thank Prof. Manfred Husty for his invaluable support and insightful comments and more specifically for recomputing and right-proofing our calculations and assumptions. The authors would like to thank his colleague Dr. Djebar Baroudi for the innumerous discussions regarding various technical issues. The authors would like also to thank two groups of students that contributed in the implementation of the Zero Gravity project: Crew 1: Aaron Dahlberg, Alpo Kuusisto, Atte Paananen, Daniel Salomäki, Eero Niklander, Eino Yrjänäinen, Emil Sevelius, Filimon Paasilahti, Jens Kruskopf, Iivo Metsä-Eerola, Sara Burke, Urho Hakonen and Crew 2: Aapo Korolainen, Eres Berki, Ivan Filimonov, Saskia Sabatini, Anastasia Luzina, Ali Akhondzada, Quentin Sola, Isabel Thelen, Mengfei Zhou, Yuxin Wu.

Appendix A

The length vector $\vec{l}^{(n)}$ of element n is defined as follows:

$$\vec{l}^{(n)} = (x_{p+6}^{(n)} - x_p^{(n)})\vec{i} + (y_{p+6}^{(n)} - y_p^{(n)})\vec{j} + (z_{p+6}^{(n)} - z_p^{(n)})\vec{k} \tag{A.1}$$

The unit vector $\vec{e}^{(n)}$ of element n is given by:

$$\vec{e}^{(n)} = \frac{\vec{l}^{(n)}}{l^{(n)}} = \frac{(x_{p+6}^{(n)} - x_p^{(n)})\vec{i} + (y_{p+6}^{(n)} - y_p^{(n)})\vec{j} + (z_{p+6}^{(n)} - z_p^{(n)})\vec{k}}{\sqrt{(x_{p+6}^{(n)} - x_p^{(n)})^2 + (y_{p+6}^{(n)} - y_p^{(n)})^2 + (z_{p+6}^{(n)} - z_p^{(n)})^2}} \tag{A.2}$$

where $l^{(n)}$ is the length of element n defined as follows:

$$l^{(n)} = |\vec{l}^{(n)}| = \sqrt{(x_{p+6}^{(n)} - x_p^{(n)})^2 + (y_{p+6}^{(n)} - y_p^{(n)})^2 + (z_{p+6}^{(n)} - z_p^{(n)})^2} \tag{A.3}$$

The position vector $\vec{r}_{1n}$ at the roof level from the top of column 1 to the top of column n, is obtained by the following expression:

$$\vec{r}_{1n} = (x_{p+6}^{(n)} - x_{p+6}^{(1)})\vec{i} + (y_{p+6}^{(n)} - y_{p+6}^{(1)})\vec{j} + (z_{p+6}^{(n)} - z_{p+6}^{(1)})\vec{k} \tag{A.4}$$

The external force vector **F** is defined as:

$$\mathbf{F} = \begin{bmatrix} 0 \\ 0 \\ P \\ -P\left((y_{p+6}^{(1)} - y_{p+6}^{(aP)})\right) \\ -P\left((x_{p+6}^{(aP)} - x_{p+6}^{(1)})\right) \\ 0 \end{bmatrix} \tag{A.5}$$

where the point aP corresponds to the point of application of the load P. The vector **X** of the unknown internal forces in the columns is defined as:

$$\mathbf{X} = \begin{bmatrix} N^{(1)} \\ N^{(2)} \\ N^{(3)} \\ N^{(4)} \\ N^{(5)} \\ N^{(6)} \end{bmatrix} \tag{A.6}$$

The matrix **A** is defined as given in Box I:

$$\mathbf{A} = \begin{bmatrix} \frac{x_p^{(1)} - x_{p+6}^{(1)}}{f^{(1)}} & \frac{x_p^{(2)} - x_{p+6}^{(2)}}{f^{(2)}} & \frac{x_p^{(3)} - x_{p+6}^{(3)}}{f^{(3)}} & \frac{x_p^{(4)} - x_{p+6}^{(4)}}{f^{(4)}} & \frac{x_p^{(5)} - x_{p+6}^{(5)}}{f^{(5)}} & \frac{x_p^{(6)} - x_{p+6}^{(6)}}{f^{(6)}} \\ \frac{y_p^{(1)} - y_{p+6}^{(1)}}{f^{(1)}} & \frac{y_p^{(2)} - y_{p+6}^{(2)}}{f^{(2)}} & \frac{y_p^{(3)} - y_{p+6}^{(3)}}{f^{(3)}} & \frac{y_p^{(4)} - y_{p+6}^{(4)}}{f^{(4)}} & \frac{y_p^{(5)} - y_{p+6}^{(5)}}{f^{(5)}} & \frac{y_p^{(6)} - y_{p+6}^{(6)}}{f^{(6)}} \\ \frac{z_p^{(1)} - z_{p+6}^{(1)}}{f^{(1)}} & \frac{z_p^{(2)} - z_{p+6}^{(2)}}{f^{(2)}} & \frac{z_p^{(3)} - z_{p+6}^{(3)}}{f^{(3)}} & \frac{z_p^{(4)} - z_{p+6}^{(4)}}{f^{(4)}} & \frac{z_p^{(5)} - z_{p+6}^{(5)}}{f^{(5)}} & \frac{z_p^{(6)} - z_{p+6}^{(6)}}{f^{(6)}} \\ 0 & \frac{\left(x_{p+6}^{(2)} - x_{p+6}^{(1)}\right)\left(z_p^{(2)} - z_{p+6}^{(2)}\right) - \left(z_{p+6}^{(2)} - z_{p+6}^{(1)}\right)\left(x_p^{(2)} - x_{p+6}^{(2)}\right)}{f^{(2)}} & \frac{\left(x_{p+6}^{(3)} - x_{p+6}^{(1)}\right)\left(z_p^{(3)} - z_{p+6}^{(3)}\right) - \left(z_{p+6}^{(3)} - z_{p+6}^{(1)}\right)\left(x_p^{(3)} - x_{p+6}^{(3)}\right)}{f^{(3)}} & \frac{\left(x_{p+6}^{(4)} - x_{p+6}^{(1)}\right)\left(z_p^{(4)} - z_{p+6}^{(4)}\right) - \left(z_{p+6}^{(4)} - z_{p+6}^{(1)}\right)\left(x_p^{(4)} - x_{p+6}^{(4)}\right)}{f^{(4)}} & \frac{\left(x_{p+6}^{(5)} - x_{p+6}^{(1)}\right)\left(z_p^{(5)} - z_{p+6}^{(5)}\right) - \left(z_{p+6}^{(5)} - z_{p+6}^{(1)}\right)\left(x_p^{(5)} - x_{p+6}^{(5)}\right)}{f^{(5)}} & \frac{\left(x_{p+6}^{(6)} - x_{p+6}^{(1)}\right)\left(z_p^{(6)} - z_{p+6}^{(6)}\right) - \left(z_{p+6}^{(6)} - z_{p+6}^{(1)}\right)\left(x_p^{(6)} - x_{p+6}^{(6)}\right)}{f^{(6)}} \\ 0 & \frac{\left(z_{p+6}^{(2)} - z_{p+6}^{(1)}\right)\left(y_p^{(2)} - y_{p+6}^{(2)}\right) - \left(y_{p+6}^{(2)} - y_{p+6}^{(1)}\right)\left(z_p^{(2)} - z_{p+6}^{(2)}\right)}{f^{(2)}} & \frac{\left(z_{p+6}^{(3)} - z_{p+6}^{(1)}\right)\left(y_p^{(3)} - y_{p+6}^{(3)}\right) - \left(y_{p+6}^{(3)} - y_{p+6}^{(1)}\right)\left(z_p^{(3)} - z_{p+6}^{(3)}\right)}{f^{(3)}} & \frac{\left(z_{p+6}^{(4)} - z_{p+6}^{(1)}\right)\left(y_p^{(4)} - y_{p+6}^{(4)}\right) - \left(y_{p+6}^{(4)} - y_{p+6}^{(1)}\right)\left(z_p^{(4)} - z_{p+6}^{(4)}\right)}{f^{(4)}} & \frac{\left(z_{p+6}^{(5)} - z_{p+6}^{(1)}\right)\left(y_p^{(5)} - y_{p+6}^{(5)}\right) - \left(y_{p+6}^{(5)} - y_{p+6}^{(1)}\right)\left(z_p^{(5)} - z_{p+6}^{(5)}\right)}{f^{(5)}} & \frac{\left(z_{p+6}^{(6)} - z_{p+6}^{(1)}\right)\left(y_p^{(6)} - y_{p+6}^{(6)}\right) - \left(y_{p+6}^{(6)} - y_{p+6}^{(1)}\right)\left(z_p^{(6)} - z_{p+6}^{(6)}\right)}{f^{(6)}} \end{bmatrix} \quad \text{(A.7)}$$

Box I.

Appendix B. Supplementary data

Supplementary material related to this article can be found online at https://doi.org/10.1016/j.engstruct.2021.113304.

References

[1] Fichter E, Kerr D, Rees-Jones J. The Gough—Stewart platform parallel manipulator: A retrospective appreciation. Proc Inst Mech Eng C 2009;223(1):243–81. http://dx.doi.org/10.1243/09544062JMES1137.

[2] Gough V, Whitehall S. Universal tyre test machine. In: Proceedings of the FISITA 9th international technical congress. 1962; p. 117–37.

[3] Stewart D. A platform with six degrees of freedom. Proc Inst Mech Eng 1965;180(1):371–86. http://dx.doi.org/10.1243/PIME_PROC_1965_180_029_02.

[4] Merlet J. Parallel robots. 2nd ed.. Springer Publishing Company, Incorporated; 2010.

[5] Bonev I. The true origins of parallel robots. 2003, http://www.parallemic.org/Reviews/Review007.html.

[6] Furqan M, Suhaib M, Ahmad N. Studies on Stewart platform manipulator: A review. J Mech Sci Technol 2017;31:4459–70.

[7] Morán E, Báez E, Aguilar E, Escobar L, Pinto N. Design of a spatial disorientation simulator using a modified Stewart-Gough platform. In: 2018 IEEE third ecuador technical chapters meeting (ETCM). 2018, p. 1–6.

[8] Copeland Z, Jung B-H, Hayes M, Langlois RG. Full-scale atlas motion platform : Structure ; actuation ; control. Int J Mech Robot Syst 2016;3:94–112.

[9] Advani S, Giovannetti D, Blum M. Design of a hexapod motion cueing system for the NASA ames vertical motion simulator. In: AIAA modeling and simulation technologies conference and exhibit. 2004, https://arc.aiaa.org/doi/abs/10.2514/6.2002-4794.

[10] Campos A, Quintero J, Saltaren R, Ferre M, Aracil R. An active helideck testbed for floating structures based on a Stewart-Gough platform. In: 2008 IEEE/RSJ international conference on intelligent robots and systems. 2008, p. 3705–10.

[11] Ross J, Seto M, Johnston C. Zero visibility autonomous landing of quadrotors on underway ships in a sea state. In: 2019 IEEE international symposium on robotic and sensors environments (ROSE). 2019, p. 1–7.

[12] Liu X, Wiersma RD. Optimization based trajectory planning for real-time 6DoF robotic patient motion compensation systems. PLOS ONE 2019;14(1):1–16. http://dx.doi.org/10.1371/journal.pone.0210385.

[13] Belcher AH, Liu X, Grelewicz Z, Pearson E, Wiersma RD. Development of a 6DOF robotic motion phantom for radiation therapy. Med Phys 2014;41(12):121704, https://aapm.onlinelibrary.wiley.com/doi/abs/10.1118/1.4900828.

[14] Akçali I, Şahlar M, Ün K, Aydın A, İbrikçi T, Esen R, Gülşen M, Bayram H. A mathematical model in the implementation of a Stewart-Gough platform as an external fixator. In: World congress on medical physics and biomedical engineering, September 7 - 12, 2009, Munich, Germany. Berlin, Heidelberg: Springer Berlin Heidelberg; 2010, p. 708–11.

[15] Paley D. History and science behind the six-axis correction external fixation devices in orthopaedic surgery. Oper Tech Orthop 2011;21(2):125–8, http://www.sciencedirect.com/science/article/pii/S1048666611000310, Deformity Correction Techniques.

[16] Sevillano G, Elias D, Callupe R, Marcacuzco R, Barriga B, Potkonjak V, Muller A. Gait simulator based on the parallel Stewart-Gough platform. In: Interdisciplinary applications of kinematics. Dordrecht: Springer Netherlands; 2011, p. 99–108.

[17] Kalani H, Moghimi S, Akbarzadeh A. Towards an SEMG-based tele-operated robot for masticatory rehabilitation. Comput Biol Med 2016;75:243–56, http://www.sciencedirect.com/science/article/pii/S0010482516301299.

[18] Yang S, Balicki M, MacLachlan R, Liu X, Kang J, Taylor R, Riviere C. Optical coherence tomography scanning with a handheld vitreoretinal micromanipulator. In: 2012 annual international conference of the IEEE engineering in medicine and biology society, EMBC 2012. Proceedings of the annual international conference of the IEEE engineering in medicine and biology society, EMBS, 2012, p. 948–51.

[19] Yang S, Wells T, MacLachlan R, Riviere C. Performance of a 6-degree-of-freedom active microsurgical manipulator in handheld tasks. In: 2013 35th annual international conference of the IEEE engineering in medicine and biology society (EMBC). 2013, p. 5670–3.

[20] Wapler M, Urban V, Weisener T, Stallkamp J, Dürr M, Hiller A. A Stewart platform for precision surgery. Trans Inst Meas Control 2003;25(4):329–34.

[21] Kobler J-P, Kotlarski J, Oltjen J, Baron S, Ortmaier T. Design and analysis of a head-mounted parallel kinematic device for skull surgery. Int J Comput Assist Radiol Surg 2011;7:137–49.

[22] Park J-H, Stegall P, Agrawal SK. Dynamic brace for correction of abnormal postures of the human spine. In: 2015 IEEE international conference on robotics and automation (ICRA). 2015, p. 5922–7.

[23] Reinoso O, Aracil R, Saltaren R. Using parallel platforms as climbing robots. In: Industrial robotics. Rijeka: IntechOpen; 2006, http://dx.doi.org/10.5772/4922.

[24] Galván-Pozos D, Ocampo-Torres F. Dynamic analysis of a six-degree of freedom wave energy converter based on the concept of the Stewart-Gough platform. Renew Energy 2020;146:1051–61, http://www.sciencedirect.com/science/article/pii/S0960148119310171.

[25] Horoub MM, Hassan M, Hawwa MA. Workspace analysis of a Gough-Stewart type cable marine platform subjected to harmonic water waves. Mech Mach Theory 2018;120:314–25, http://www.sciencedirect.com/science/article/pii/S0094114X1630708X.

[26] Keshtkar S, Poznyak A, Hernandez E, Oropeza A. Adaptive sliding-mode controller based on the "Super-Twist" state observer for control of the Stewart platform. Autom Remote Control 2017;1218–33.

[27] Jáuregui JC, Hernández EE, Ceccarelli M, López-Cajún C, García A. Kinematic calibration of precise 6-DOF stewart platform-type positioning systems for radio telescope applications. Front Mech Eng 2013;8(3):252, http://journal.hep.com.cn/fme/EN/abstract/article_4629.shtml.

[28] Yingjie L, Wenbai Z, Gexue R. Feedback control of a cable-driven gough-stewart platform. IEEE Trans Robot 2006;22(1):198–202.

[29] Qian Z, Hui Z. Simulation and experimental analysis of the Stewart parallel mechanism for vibration control. In: SMC'03 conference proceedings. 2003 IEEE international conference on systems, man and cybernetics. Conference theme - System security and assurance (Cat. No.03CH37483), Vol. 4. 2003, p. 3548–52.

[30] Preumont A, Horodinca M, Romanescu I, de Marneffe B, Avraam M, Deraemaeker A, Bossens F, Hanieh AA. A six-axis single-stage active vibration isolator based on Stewart platform. J Sound Vib 2007;300(3):644–61, http://www.sciencedirect.com/science/article/pii/S0022460X06007334.

[31] Hanieh AA, Preumont A. Active isolation and damping of vibrations via stewart platform. 2003.

[32] Hauge G, Campbell M. Sensors and control of a space-based six-axis vibration isolation system. J Sound Vib 2004;269(3):913–31, http://www.sciencedirect.com/science/article/pii/S0022460X03002062.

[33] Iqbal S, Bhatti A, Ahmed Q. Dynamic analysis and robust control design for Stewart platform with moving payloads. IFAC Proc Vol 2008;41(2):5324–9, http://www.sciencedirect.com/science/article/pii/S1474667016397907.

[34] Richter T, Lorenc SJ, Bernold LE. Cable based robotic work platform for construction. In: Proceedings of the 15th ISARC. 1998.

[35] Salah B, Ramadan M, Noche B. Travel time analysis of Stewart-Gough platform in automated storage and retrieval system. In: 2011 IEEE international conference on automation and logistics (ICAL). 2011, p. 143–8.

[36] Lalo W, Bruckmann T, Schramm D. Optimal control for a wire-based storage retrieval machine. In: Viadero F, Ceccarelli M, editors. New trends in mechanism and machine science. Mechanisms and machine science, vol. 7, 2013.

[37] Kim K-T, Bernold LE. A comparison of two innovative technologies for safe pipe installation — "Pipeman" and the Stewart–Gough platform-based pipe manipulator. Autom Constr 2008;17(3):322–32, http://www.sciencedirect.com/science/article/pii/S092658050700074X, 8th International Conference on Computer-Aided Engineering.

[38] Fry ST, Turner CJ. Design of a Stewart-Gough platform for engineering material characterization. ASME international mechanical engineering congress and exposition, 2016, http://dx.doi.org/10.1115/IMECE2016-66669.

[39] Zhang D, Gao Z, Hu X, Parise J. Novel design of a 3-DOF parallel manipulator for materials handling. International design engineering technical conferences and computers and information in engineering conference, 2008, p. 719–26. http://dx.doi.org/10.1115/DETC2008-49188.

[40] Hansen AB, Laursen JM, Henriksen ST, Ringgaard K, Rydahl-Haastrup M, Balling O. Calibration of reconfigurable Stewart-Gough platform for mobile machining application. International design engineering technical conferences and computers and information in engineering conference, 2019, http://dx.doi.org/10.1115/DETC2019-98137, V05BT07A015.

[41] Filz GH, Elmas S, Markou AA. Zero-gravity 2.0 exhibition. 2019, https://www.aalto.fi/en/research-art/zero-gravity-20-exhibition.

[42] Husty M. An algorithm for solving the direct kinematics of general Stewart-Gough platforms. Mech Mach Theory 1996;31(4):365–79, https://search.datacite.org/works/10.1016/0094-114x(95)00091-c.

[43] Dasgupta B, Mruthyunjaya T. The Stewart platform manipulator: a review. Mech Mach Theory 2000;35(1):15–40, https://www.sciencedirect.com/science/article/pii/S0094114X99000063, ID: 271468.

[44] Bandyopadhyay S, Ghosal A. An algebraic formulation of kinematic isotropy and design of isotropic 6-6 Stewart platform manipulators. Mech Mach Theory 2008;43(5):591–616, https://www.sciencedirect.com/science/article/pii/S0094114X07001036, ID: 271468.

[45] Bessala J, Bidaud P, Ouezdou F. Analytical study of stewart platform workspaces, Vol. 4. 1996, p. 3179–84.

[46] Shastry S, Avaneesh R, Desai K, Shah S. Optimal design of a Stewart–Gough platform for multidirectional 3-D printing. In: Precision product-process design and optimization. Singapore: Springer Singapore; 2018, p. 1–29, ID: http://dx.doi.org/10.1007/978-981-10-8767-71.

[47] Gosselin C, Merlet J-P. Parallel robots: Architecture, modeling, and design. Encyclopedia of robotics, Berlin, Heidelberg: Springer Berlin Heidelberg; 2020, p. 1–6.

[48] Stevenson C. Kinetic architecture: Designing with movement. Birkhäuser; 2012, p. 176.

[49] Teuffel P. Entwerfen adaptiver Strukturen. 2004.

[50] Teuffel P. Optimization of adaptive structures. IABSE Symp Rep 2004;88:1–6.

[51] Habraken A, Sleddens W, Teuffel P. Adaptable lightweight structures to minimise material use. 2013, p. 71–82.

[52] Graefe R. Velaerunt : die Zeltdacher der romischen Theater und ahnlicher Anlagen. 1976, p. 221, http://catalogue.bnf.fr/ark:/12148/cb35639565v.

[53] Starr SF. Melnikov: Solo architect in a mass society. Princeton University Press; 1978, p. 276.

[54] Sascha Hendel archINFORM. Leningrad Pravda, Moskau. 2021, https://deu.archinform.net/projekte/9857.htm.

[55] Nextroom-Architektur. GucklHupf, Hans Peter Worndl - Mondsee (A) - 1993. 2003, https://www.nextroom.at/building.php?id=2623.

[56] Michelson A. Seattle World's Fair, Space Needle, Seattle, WA. (Pacific Coast Architecture Database), http://pcad.lib.washington.edu/building/4565/, Pacific Coast Architecture Database (PCAD) — 2005-2021 Alan Michelson.

[57] DRMM, de Rijke Marsh Morgan Architects. Sliding house: A house for all seasons. 2009, https://drmm.co.uk/projects/.

[58] LOT-EK architecture design. MDU - Mobile Dwelling Unit. 2003, https://lot-ek.com/MDU-Mobile-Dwelling-Unit.

[59] Edge Design Institute. Domestic transformer. 2007, https://www.edgedesign.com.hk/2007domestictransformer.

[60] Mical T. Surrealism and architecture. Psychology Press; 2005.

[61] Randl C. Revolving architecture : A history of buildings that rotate, swivel, and pivot. Princeton Architectural Press; 2008, p. 208.

[62] Nouvel J. Institut du monde arabe (IMA). 1987, http://www.jeannouvel.com/projets/institut-du-monde-arabe-ima/.

[63] Cilento K. Al bahar towers responsive facade / aedas. 2012, https://www.archdaily.com/270592/al-bahar-towers-responsive-facade-aedas.

[64] WikiArquitectura. Al bahar towers - Data, photos plans. 2012, https://en.wikiarquitectura.com/building/al-bahar-towers/.

[65] Attia S. Evaluation of adaptive facades: The case study of Al Bahr Towers in the UAE. QSci Connect 2018;2017(2). http://www.qscience.com/doi/full/10.5339/connect.2017.qgbc.6.

[66] Matin NH, Eydgahi A. Technologies used in responsive facade systems: a comparative study. Null 2019;1–20. http://dx.doi.org/10.1080/17508975.2019.1577213.

[67] Jofre Roca arquitectes. Social pavilion at an olympic shooting range. 2006, https://www.jofreroca.com/sports-club.

[68] Azzarello N. Kinetic snowcone winter station reimagines lifeguard post on toronto beach. 2015, https://www.designboom.com/architecture/snowcone-winter-stations-raw-design-ferris-curio-toronto-kew-beach-02-35-2015/.

[69] Pasquini M. Shiver Pavilion: Kinetic architecture in Finland. A pavilion for a relationship between man and nature. 2020, https://www.arkitectureonweb.com/en/web/designonweb/-/kinetic-architecture-in-finland-a-pavilion-for-a-relationship-between-man-and-nature.

[70] Bajçinovci B, Aliu V, cinovci BB, Bajçinovci U. Interactive-kinetic-architecture-progressive-design-principles. 2019.

[71] Li Z, Nawratil G, Rist F, Hensel M. Invertible paradoxic loop structures for transformable design. Comput Graph Forum 2020;39(2):261–75, https://onlinelibrary.wiley.com/doi/abs/10.1111/cgf.13928.

[72] Calatrava S. Zur faltbarkeit von fachwerken (Ph.D. thesis), 1981, http://dx.doi.org/10.3929/ethz-a-000240711.

[73] Hoberman C. Hoberman associates – Transformable design. 1990, https://www.hoberman.com/.

[74] Pietroni N, Tarini M, Vaxman A, Panozzo D, Cignoni P. Position-based tensegrity design. ACM Trans Graph 2017;36(6):1–14, http://dl.acm.org/citation.cfm?id=3130809.

[75] Vergauwen A, Temmerman N. Analysing the applicability of deployable scissor structures in responsive building skins. 2012, p. 493–504.

[76] Zheng C, Sun T, Chen X. Deployable 3D linkages with collision avoidance. SCA 16, Eurographics Association; 2016, p. 179–88, http://dl.acm.org/citation.cfm?id=2982843.

[77] Ryssy J, Natarajan AK, Wang J, Lehtonen AJ, Nguyen M-K, Klajn R, Kuzyk A. Light-responsive dynamic DNA-origami-based plasmonic assemblies. Angew Chem Int Ed 2021;60(11):5859–63. http://dx.doi.org/10.1002/anie.202014963.

[78] Gehry FO, Ahrendt E, von Vegesack A. Frank O. Gehry: Design architecture - Gehry Milunic: The dancing house. Weil am Rhein: Vitra-Design-Museum; 1996.

[79] Zaha Hadid Architects. Vitra fire station – Zaha hadid architects. 1993, https://www.zaha-hadid.com/architecture/vitra-fire-station-2/.

[80] de Haas Architectures AX. Aluminium forest. Building with water: Concepts typology design, Basel: Birkhäuser; 2012, p. 82–7, https://www.degruyter.com/document/doi/10.1515/9783034610940.82/html.

[81] Wallraff M. Infobox vienna central station. 2011, http://www.wallraff.at/detail.php?xp=082.

[82] Filz GH, Naicu D. "2 Landscapes" - interaction of 2 gridshells based on a modified Stewart-Gough principle. In: IASS WORKING GROUPS 12 and 18 international colloquium 2015 bio-based and bio-inspired environmentally compatible structures. IASS; 2015, http://opus.bath.ac.uk/47846.

[83] Filz GH. cut.enoid.tower [kʌt.ənɔɪd.taʊər]. In: Bögner-Balz, Heidrun; Mollaert, Marijke; Pusat, Emre: Proceeding tensinet symposium 2013. 2013, p. 577–84.

[84] Filz GH. Low-tech or High-tech? "cut.enoid.tower" - three times two facets of irregularity. In: VI international conference on textile composites and inflatable structures (Structural membranes 2013). Barcelona: CIMNE; 2013, p. 250–7.

[85] Schaur E, Filz GH, Hartmann MF, Maleczek R, Mössmer G, Sack F. Konstruktion und Gestaltung: Neue formwelten für architektur. Innsbruck, Austria: Innsbruck Univ. Press; 2013, p. 278.

[86] Parasonis J, Jodko A. Architectural engineering as a profession: Report on research leading to a curriculum revision. J Civ Eng Manage 2013;19:738–48.

[87] Larsen OP, Tyas A. Conceptual structural design: Bridging the gap between architects and engineers. Thomas Telford Publishing; 2003, p. 134. http://dx.doi.org/10.1680/csdbtgbaae.32354, 14.

[88] Moe K. Integrated design in contemporary architecture. Princeton Architectural Press; 2008.

[89] Coros S, Thomaszewski B, Noris G, Sueda S, Forberg M, Sumner R, Matusik W, Bickel B. Computational design of mechanical characters. ACM Trans Graph 2013;32(4):1–12, http://dl.acm.org/citation.cfm?id=2461953.

[90] Lin M, Mandocha D, Kim Y. Collision and proximity queries. Handbook of discrete and computational geometry, 3rd ed.. Boca Raton, FL, USA: CRC Press; 2017, p. 1029–56, ch. 39.

[91] Durmus Ozturk S. Rethinking the black box in architecture design studio. SAGE Open 2020. http://dx.doi.org/10.1177/2158244020927408.

[92] Elblaus L, Hansen KF, Unander-Scharin C. Artistically directed prototyping in development and in practice. J New Music Res 2012;41(4):377–87. http://dx.doi.org/10.1080/09298215.2012.738233.

[93] Elmas S, Filz GH, Markou AA. Zero Gravity: a novel cantilever beam utilizing elastic torsion for structures and architecture. In Proceedings of IASS Annual Symposia. International Association for Shell and Spatial Structures (IASS), Surrey, UK; 2021.

[94] Arduino A. Arduino. 2020, https://www.arduino.cc/.

[95] Timoshenko S, Young D. Theory of structures. McGraw-Hil; 1965.

[96] MATLAB version 9.8.0.1380330 (R2020a). Natick, Massachusetts: The Mathworks, Inc.; 2020.

[97] Grasshopper. Seattle, WA: McNeel, Robert and Associates; 2020, https://www.grasshopper3d.com.

[98] Rhinoceros 3D, Version 6.0. Seattle, WA: McNeel, Robert and Associates; 2010.

[99] Piker D. Kangaroo: form finding with computational physics. Archit Des 2013;83(2):136–7.

[100] Deo S, Hölttä-Otto K, Filz GH. Creativity and engineering education: Assessing the impact of a multidisciplinary project course on engineering students' creativity. In: ASME 2020 international design engineering technical conferences and computers and information in engineering conference. American Society of Mechanical Engineers; 2020, https://asmedigitalcollection.asme.org/IDETC-CIE/proceedings/IDETC-CIE2020/83921/Virtual.

[101] Filz GH, Elmas S, Markou AA, Hölttä-Otto K, Deo S. Zero Gravity : radical creativity by multidisciplinary collaboration. In Proceedings of IASS Annual Symposia. International Association for Shell and Spatial Structures (IASS), Surrey, UK; 2021.

[102] Henry W. Return of the master builder. 2012, p. 422.

[103] Billington DP, Garlock MM. Thin shell concrete structures: The master builders. J Int Assoc Shell Spat Struct 2004;45(146):147–55.